© 2019. Published by The Company of Biologists Ltd | Development (2019) 146, dev171579. doi:10.1242/dev.171579

RESEARCH ARTICLE

Dual control of Kinesin-1 recruitment to microtubules by Ensconsin in *Drosophila* neuroblasts and oocytes

Mathieu Métivier[1], Brigette Y. Monroy[3], Emmanuel Gallaud[1], Renaud Caous[1], Aude Pascal[1], Laurent Richard-Parpaillon[1], Antoine Guichet[2], Kassandra M. Ori-McKenney[3] and Régis Giet[1,*]

ABSTRACT

Drosophila Ensconsin (also known as MAP7) controls spindle length, centrosome separation in brain neuroblasts (NBs) and asymmetric transport in oocytes. The control of spindle length by Ensconsin is Kinesin-1 independent but centrosome separation and oocyte transport require targeting of Kinesin-1 to microtubules by Ensconsin. However, the molecular mechanism used for this targeting remains unclear. Ensconsin contains a microtubule (MT)-binding domain (MBD) and a Kinesin-binding domain (KBD). Rescue experiments show that only full-length Ensconsin restores the spindle length phenotype. KBD expression rescues *ensc* centrosome separation defects in NBs, but not the fast oocyte streaming and the localization of Staufen and Gurken. Interestingly, the KBD can stimulate Kinesin-1 targeting to MTs *in vivo* and *in vitro*. We propose that a KBD and Kinesin-1 complex is a minimal activation module that increases Kinesin-1 affinity for MTs. Addition of the MBD present in full-length Ensconsin allows this process to occur directly on the MT and triggers higher Kinesin-1 targeting. This dual regulation by Ensconsin is essential for optimal Kinesin-1 targeting to MTs in oocytes, but not in NBs, illustrating the importance of adapting Kinesin-1 recruitment to different biological contexts.

KEY WORDS: Ensconsin, Kinesin-1, Microtubule, *Drosophila*, Neuroblast, Oocyte

INTRODUCTION

Microtubules (MTs) are dynamic polymers that grow and shrink over time, a process known as dynamic instability (Mitchison and Kirschner, 1984). They are regulated by microtubule-associated proteins (MAPs), which have a wide range of activities. MAPs can modify microtubule dynamic parameters, and are able to organize microtubules into complex structures. The MAP family also includes microtubule motors that slide along the MTs. These motor proteins use ATP hydrolysis to move cargo along microtubules, thus transporting vesicles, chromosomes, proteins, RNA and even other microtubules. MT networks and their associated MAPs therefore play key roles in various biological processes, including cell division, intracellular trafficking and cell morphogenesis (Barlan and Gelfand, 2017; Heald and Khodjakov, 2015; Walczak and Heald, 2008).

[1]Univ. Rennes, CNRS, IGDR (Institut de Génétique et Développement de Rennes) - UMR 6290, F-35000 Rennes, France. [2]Institut Jacques Monod-Université Paris Diderot-Paris 7, 15 rue Hélène Brion, 75205 Paris Cedex 13, France. [3]University of California, Davis, One Shields Avenue, Davis, CA 95616, USA.

*Author for correspondence (regis.giet@univ-rennes1.fr)

A.G., 0000-0001-7216-1944; K.M.O., 0000-0003-2051-2495; R.G., 0000-0001-9027-5849

Received 6 September 2018; Accepted 25 March 2019

Ensconsin (also known as MAP7) was first identified in microtubule preparations isolated from epithelial cells (Bulinski and Bossler, 1994). The protein has been given several names, including epithelial MAP of 115 kDa (E-MAP115) and Ensconsin, owing to its tenacious association with microtubules both *in vivo* and *in vitro* (Bulinski and Bossler, 1994). Ensconsin is associated with the interphase microtubule cytoskeleton, but its overexpression in cultured cells does not seem to affect microtubule dynamics during interphase, and instead mitotic abnormalities frequently occur during cell division (Faire et al., 1999).

The possible function of Ensconsin remained elusive for a decade, until *ensc* mutant flies were isolated in a screen for genes affecting *Drosophila* female germline development. *ensc* mutant females are sterile, and oocytes display microtubule-dependent mislocalization of several polarized key molecules required for the proper patterning of developing embryos. These molecules include *oskar* mRNA and its binding partner, the Staufen adaptor protein, on the posterior side (Ferrandon et al., 1994; St Johnston et al., 1991; Sung et al., 2008), and the Gurken protein, a TGFβ-like ligand, on the dorso-ventral axis (Neuman-Silberberg and Schupbach, 1993; Sung et al., 2008). The *ensc* mutant oocytes also show absent microtubule-dependent streaming of granules (Sung et al., 2008). Interestingly, these defects are shared by Kinesin heavy chain (KHC) mutants (Brendza et al., 2000, 2002; Duncan and Warrior, 2002; Januschke et al., 2002). In *ensc* oocyte extracts, the recruitment of Kinesin-1 motors to MTs is impaired *in vitro*, and it has recently been shown that purified Ensconsin proteins can directly recruit Kinesin-1 to the MT *in vitro*, providing evidence for a model in which Ensconsin stimulates recruitment of Kinesin-1 to MTs (Sung et al., 2008). This recruitment model is also evident in mouse and *Drosophila* muscle cells. In these large cells, both Ensconsin and Kinesin-1 are required to promote nuclei positioning and spacing, processes that are required for correct muscle function. In this study, the authors also showed a direct physical association between the Kinesin-1 motor and the Ensconsin C-terminal domain (the Kinesin-binding domain, or KBD). Furthermore, after Kinesin-1 or Ensconsin knockdown, a fusion between the Ensconsin N-terminal MT-binding domain (MBD) and the Kinesin-1 motor domain is sufficient to rescue nucleus-positioning defects (Metzger et al., 2012). Together, the studies of muscle cells and fly oocytes cited here support a model in which Ensconsin favours Kinesin-1 microtubule recruitment via its MBD and KBD domains (Metzger et al., 2012; Sung et al., 2008). However, a second model, based on S2 cultured cell studies, proposes that some Ensconsin function does not depend on the MBD. For these functions, Kinesin-1 can be recruited solely by the KBD (Barlan et al., 2013), showing that microtubule targeting by Ensconsin is not an absolute requirement for Kinesin-1 function. Here, we have used a combination of genetic studies with rescue constructs at different stages of fly development, as well as *in vitro* experiments, to unambiguously show that

Development (2019) 146, dev171579. doi:10.1242/dev.171579

Kinesin-1 is actually subjected to dual recruitment by Ensconsin that synergizes its loading onto microtubules.

RESULTS

In vivo functional analysis of the different domains of Ensconsin

A previous study identified two Ensconsin deletion mutants, named *enscΔNull* and *enscΔN*, expressing, respectively, no protein or with the C-terminal Kinesin-binding domain intact (Sung et al., 2008). However, western blotting analyses showed that these two mutants do not express detectable Ensconsin protein or truncated products, and are therefore null alleles (see Materials and Methods for details, and Gallaud et al., 2014). To investigate the roles of the Ensconsin functional domains (microtubule binding and kinesin binding), we generated several fly lines. These expressed full-length Ensc-GFP, Ensc-MBD-GFP or Ensc-KBD-GFP, under the control of the poly-ubiquitin promoter. These lines were then used for rescue experiments in *ensc* mutant flies (Fig. 1A, and Materials and Methods). We used western blots to monitor the expression of the GFP-tagged Ensconsin variants in brain extracts. The exogenous full-length Ensc-GFP appeared as a 150 kDa doublet in western blots, and it was expressed at levels similar to those of endogenous Ensconsin (Fig. 1B, middle panel, lanes 6 and 7). The MBD-GFP (Fig. 1B, top panel, lanes 2 and 3) and KBD-GFP (lane 5) proteins, appeared as 70 and 100 kDa bands, respectively, and were expressed at similar levels to Ensc-GFP (lane 7). In *ensc* mutant flies, Ensc-GFP expression rescued the partial lethality and restored female fertility. However, the expression of MBD-GFP, as tested in three independent transgenic lines, failed to do so. In contrast, in two independent lines, KBD-GFP expression in *ensc*-null mutant flies rescued the partial lethality as much as wild-type Ensc-GFP, which suggests that this domain is sufficient for fly development into adulthood. However, we noticed that the Ensc-KBD female flies remained sterile, suggesting that the KBD alone is not enough to fully restore some aspects of oocyte development. To show that Ensconsin was able to physically interact with Kinesin-1, we performed immunoprecipitation experiments using whole female fly extracts expressing the GFP-tagged proteins (see Materials and Methods, and Fig. 1C, top panel). We found that both Ensc-GFP and KBD-GFP, but not MBD-GFP, proteins were able to interact with KHC (Fig. 1C, bottom panel), similarly to vertebrate Ensconsin (MAP7) (Hooikaas et al., 2019; Metzger et al., 2012).

The Ensconsin KBD fully rescues Kinesin-dependent centrosome separation defects in fly neuroblasts

A previous study has shown that Ensconsin stimulates microtubule growth during mitosis. Consequently, *ensc* mitotic spindles are 20% shorter than their wild-type counterparts in neural stem cells (neuroblasts, NBs) (Gallaud et al., 2014). In addition, overexpression of Ensconsin (Ensc OE) in brain neuroblasts triggers the formation of longer and bent mitotic spindles (Fig. S1). The fly NB divides asymmetrically to generate a renewing NB and a

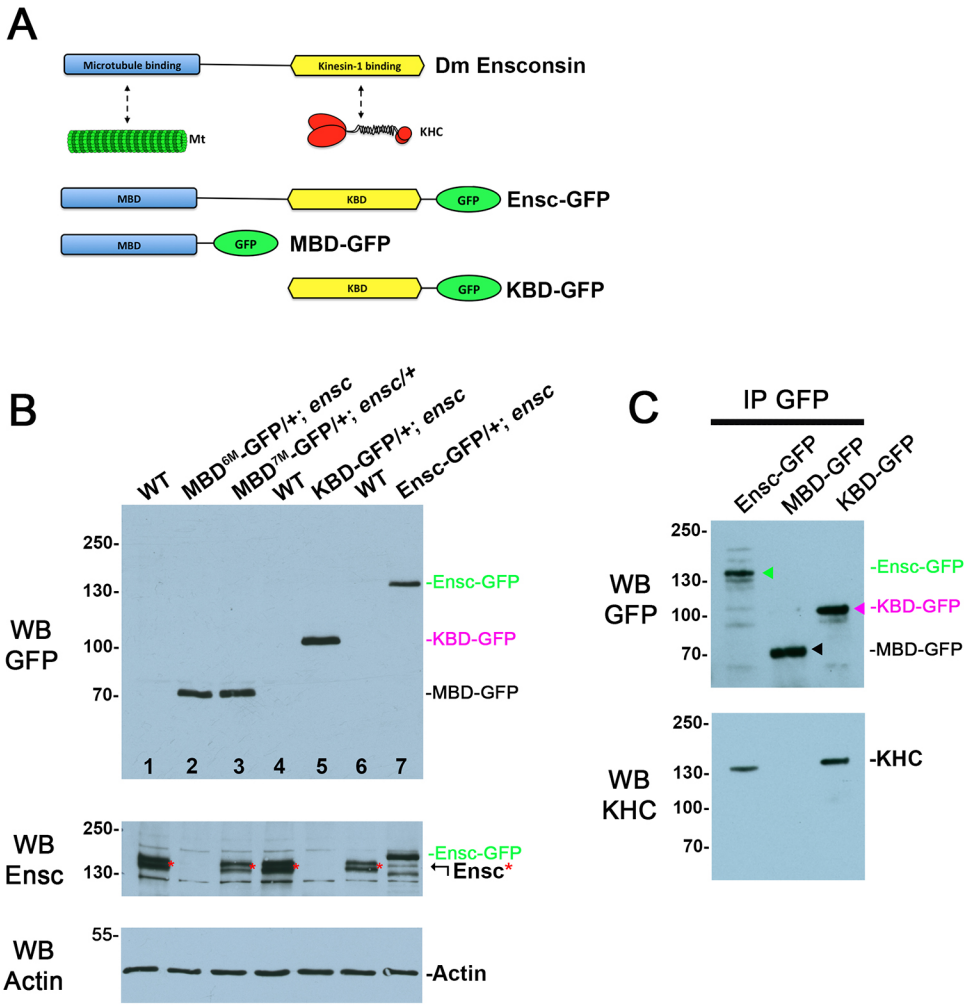

Fig. 1. Schematic diagram and expression of GFP-tagged Ensconsin variants. (A) Endogenous Ensconsin harbours an N-terminal MT-binding domain (MBD, blue) and a C-terminal Kinesin-binding domain (KBD, yellow). The three protein variants were tagged with GFP and expressed in *ensc*-null flies using a poly-ubiquitin promoter. (B) Western blot analysis of different GFP-tagged Ensconsin variants from brain tissue. The whole membrane was probed with GFP antibodies for western blotting (top). The same membrane was subsequently stripped (see Materials and Methods) to reveal endogenous Ensconsin (red asterisks) and an Actin loading control (bottom). WT, control brain tissue (lanes 1, 4, 6). The expression of the transgenes is shown in *ensc*-null individuals (lanes 2, 5, 7), except in lane 3, where a MBD-GFP line is examined in hemizygous *ensc* tissue. The endogenous Ensconsin band/doublet is indicated with a red asterisk (middle panel). (C) Whole-fly extracts were prepared and subjected to immunoprecipitation using GFP-TRAP beads (see Materials and Methods). The beads were then analysed by western blotting and probed using anti-GFP (top) or anti-KHC (bottom) antibodies. The positions of MBD-GFP, KBD-GFP and Ensc-GFP are indicated on the right with black, pink and green arrowheads, respectively. KHC is present in Ensc-GFP and KBD-GFP but not in MBD-GFP immunoprecipitates.

Development (2019) 146, dev171579. doi:10.1242/dev.171579

smaller cell subjected to differentiation. In this cell type, centrosome separation is initiated after the mother centrosome loses its MT nucleation potential. As a consequence, it is inherited in the differentiating cell, while the new centrosome retains MT nucleation and stays in the renewing NB (Conduit and Raff, 2010; Gallaud et al., 2014; Januschke et al., 2011; Rebollo et al., 2007; Rusan and Peifer, 2007). Ensconsin and Kinesin-1 are both required during interphase to promote centrosome separation in NBs. In *ensc* and khc^{27}/khc^{63} hypomorphic mutants, the centrosome separation does not occur after cytokinesis, but instead just before mitosis, leading to frequent mis-segregation of mother and daughter centrosomes (Gallaud et al., 2014). To challenge for a possible cooperation between Ensconsin and Kinesin-1, we analysed centrosome separation in khc^{27}/khc^{63} hypomorphic NBs after Ensc OE. We found Ensc OE completely rescued the centrosome separation defects in *khc* mutant neuroblasts, indicating that Ensc OE was able to boost the low Kinesin-1 activity of this hypomorphic khc^{27}/khc^{63} mutant. By contrast, *khc* mutations did not trigger spindle shortening of the long and bent spindles obtained following Ensc OE, in agreement with the fact that the regulation of the NB spindle length is a Kinesin-1 independent process (Gallaud et al., 2014, Fig. S1A-D and Movies 1-4). Importantly, KHC protein levels were normal in *ensc* mutants, and vice versa, indicating that the stability of one protein was independent upon the presence of the other (Fig. S1F). In addition, Ensconsin-Venus and endogenous Ensconsin localization (Fig. S1G,E) were not affected in a *khc* background. This indicates that Ensconsin protein stability and Ensconsin localization are Kinesin-1 independent, but that Ensconsin OE can stimulate low Kinesin-1 activity.

In parallel, we measured the angles between the two centrosomes shortly before the nuclear envelope breakdown (NEBD), as a readout of centrosome separation. In agreement with cooperation between Kinesin-1 and Ensconsin during interphase, we found that elevating the levels of Ensconsin protein (Ensconsin Overexpression: Ensc OE) completely rescued the centrosome separation defects in *khc* mutant neuroblasts, indicating that Ensc OE was able to boost the low Kinesin-1 activity of khc^{27}/Khc^{63} mutant. By contrast, *khc* mutations did not trigger spindle shortening of the long and bent spindles obtained following Ensc OE, in agreement with previous observations indicating that spindle length is independent of Kinesin-1 activity (Gallaud et al., 2014, Fig. S1A-D and Movies 1-4).

We then monitored the ability of GFP-tagged Ensconsin variants to rescue spindle length and centrosome separation defects observed in *ensc* mutants. To do this, we used live microscopy on Ensc-GFP, KBD-GFP and MBD-GFP variants co-expressing RFP-tubulin. In control NBs (Fig. 2A,F-H, Movie 5), the centrosomes were fully separated before NEBD, as the angle between the two centrosomes and the nucleus centre was between 120 and 180° (100%, n=30). In *ensc* mutants (Fig. 2B,F-H, Movie 6), most cells displayed incomplete centrosome separation before mitosis, as most of the angles between the two centrosomes and the nucleus centre were between 60 and 120° (61.9%, n=21), but this defect was restored by Ensc-GFP expression, after which 100% (n=19) of the NBs showed pre-NEBD centrosome separation that was comparable with the control (Fig. 2C,G,H, Movie 9). *ensc* mutant NBs expressing MBD-GFP showed centrosome separation defects similar to those of the *ensc* mutants (58.8% between 60 and 120°, n=17, Fig. 2D,F-H, Movie 7). *In* ensc mutant NBs expressing KBD-GFP, centrosome separation was restored (87% above 120°, n=23), suggesting that this domain can efficiently rescue the centrosome separation defects on its own (Fig. 2E,F-H, Movie 8). Interestingly, this rescue of the centrosome-separation defect did not require microtubule binding, as the KBD was not detected on MTs in squashed preparations (Fig. 2E, middle panels).

Efficient mitotic spindle assembly was assayed using spindle length measurements. Ensc variant rescue of mitotic spindle length associated with Ensconsin deletion indicated that only Ensc-GFP, and not Ensc-KBD or Ensc-MBD, was able to restore normal spindle size. This demonstrates that mitotic spindle length control in neuroblasts requires full-length Ensconsin, and that MBD-GFP and KBD-GFP are unable to restore correct spindle length individually (Fig. 2I and Movies 5-9).

The Ensconsin KBD is not sufficient for ooplasmic streaming and the correct targeting of Staufen and Gurken in the oocyte

A previous study has shown that Ensconsin is required for Staufen and Gurken transport in the oocyte to the posterior and the antero-dorsal regions, respectively (Sung et al., 2008).

We first checked that the MBP-GFP, KBD-GFP and Ensc-GFP proteins were expressed in oocytes using live immunofluorescence analyses and western blotting of oocyte extracts (see Materials and Methods for details and Fig. S4A,B).

We then monitored the localization of Gurken in *ensc* mutant oocytes expressing Ensc-GFP, KBD-GFP or MBD-GFP at stages 9 (Fig. S2). In most wild-type (71%, n=14) and Ensc-GFP oocytes (72%, n=18), Gurken was tightly localized at the cortical antero-lateral corner (Fig. S2A, top, Fig. S2C). By contrast, the majority of, *ensc* (70% n=23) and Ensc-MBD (81%, n=15) oocytes contained Gurken protein in a punctiform pattern spread around the nuclear region (Fig. S2A, bottom panels, Fig. S2B,C). KBD-GFP oocytes had an intermediate phenotype and half of these oocytes showed abnormal or incomplete Gurken localization (52%, n=12/23, Fig. S2).

At the same time, we also monitored the localization of Staufen at the posterior cell cortex (Fig. 3). During oogenesis, two Kinesin-1-dependent pathways are used to transport Staufen particles to the posterior pole of the embryo, where Myosin V captures them. At stage 9, Staufen is transported directly by Kinesin-1 through the network of polarized microtubules, the plus ends of which are directed towards the posterior cortex (Fig. 3D, top left see also Lu et al., 2018, 2016). At stage 10B, Staufen particles are transported via ooplasmic streaming: a fast and important movement of particles on mobile microtubules that slide on a population of stable microtubules that are anchored to the cortex of the ovarian chamber (Lu et al., 2018, 2016).

At stage 9, we found that Ensc-GFP (Fig. 3Ae, n=9) was able to fully rescue the cortical posterior localization of Staufen similar to the controls (Fig. 3Aa, n=13). In contrast, both in *ensc* (Fig. 3Ac, n=5) mutant oocytes and in those in which MBD-GFP was expressed (Fig. 3Ag, n=8), Staufen displayed a crescent intensity that was about five times weaker than that of wild type (Fig. 3B). Expression of KBD in *ensc* mutant oocytes (n=17) allows Staufen to be targeted to the posterior pole in stage 9 oocytes, and the crescent intensities reached 74% of the control values, although the protein appeared mislocalized in some case (Fig. 3Ai, red arrow, Fig. 3B). At stage 10B, Ensc-GFP (n=13) and wild-type (n=15) oocytes showed a normal Staufen crescent at the posterior pole (Fig. 3A, compare b with f), whereas the intensity was weak in *ensc* (Fig. 3Ad, n=11) and MBD oocytes (Fig. 3Ah, n=9). KBD oocytes (Fig. 3J, n=14) showed an intermediate phenotype and the Staufen crescent intensity was 50% of the value observed in controls (Fig. 3Aj and Fig. 3C). Because Kinesin-1-dependent ooplasmic streaming participates in Staufen targeting to the posterior cortex in stage 10B oocytes, we

Development (2019) 146, dev171579. doi:10.1242/dev.171579

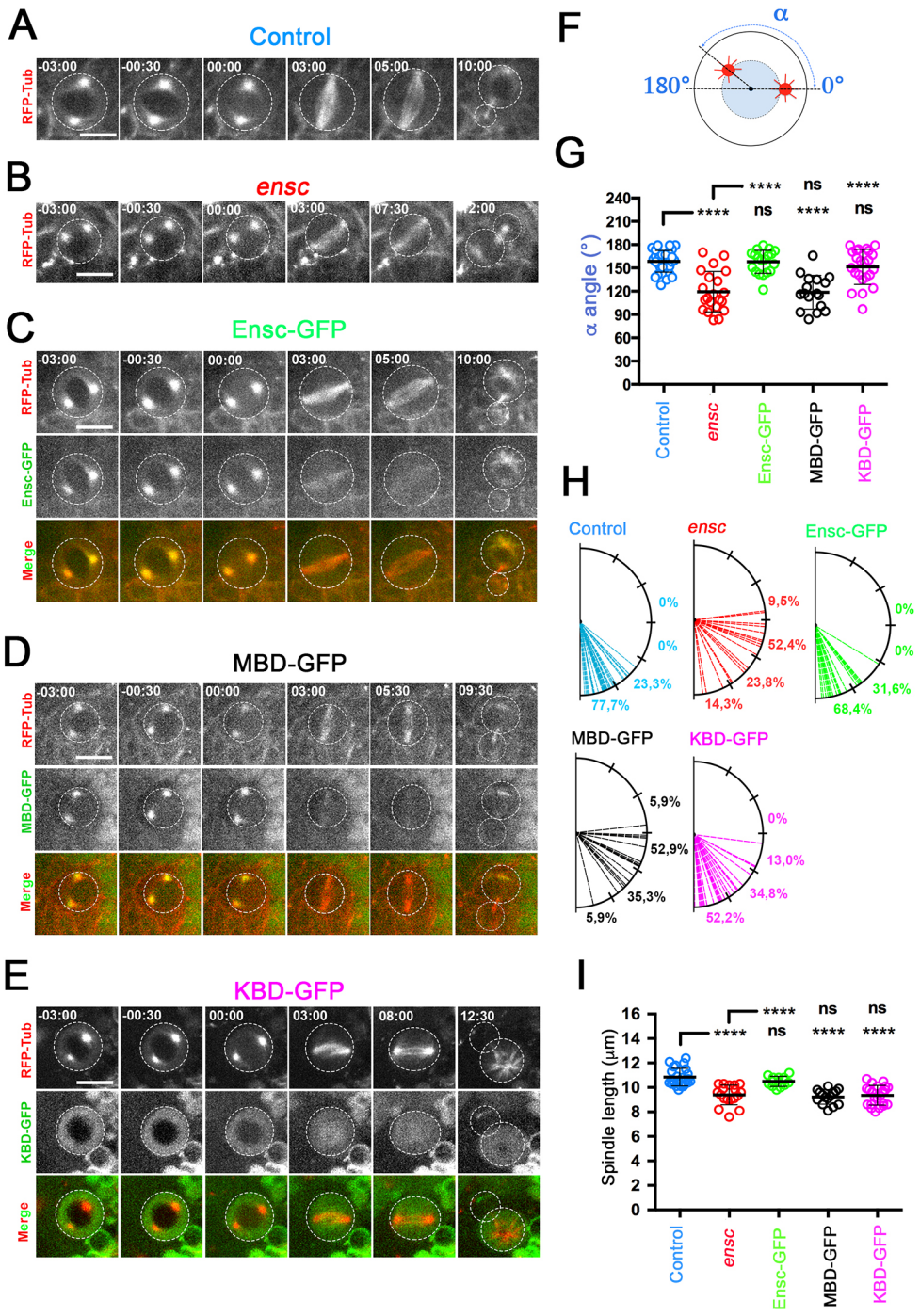

Fig. 2. Functional analysis of Ensconsin microtubule- and Kinesin-binding domains during cell division. (A,B) Selected frames of a control NB (A) and a mutant *ensc* NB (B) expressing RFP-tubulin during cell division. Thirty seconds before the nuclear envelope breakdown (NEBD), the centrosomes are already fully separated and well positioned in wild-type cells, but not in *ensc*. (C) An *ensc* mutant NB expressing Ensc-GFP during cell division. In the merged images in C-E, RFP-tubulin (RFP-Tub) is red and GFP-tagged proteins are green, whereas they are both monochrome in the top and middle panels, respectively. (D) *ensc* mutant NBs expressing MBD-GFP during cell division. Here, the centrosomes are incompletely separated before NEBD. (E) An *ensc* mutant NB expressing KBD-GFP during cell division. This particular cell was isolated from flattened brains in PBS to reveal that KBD-GFP does not colocalize with the MT cytoskeleton. The centrosome separation defect is fully restored. Scale bars: 10 µm. (F) Scheme showing the α angle measurement, reflecting centrosome separation for the indicated genotypes (see Materials and Methods). (G) Box plot showing the mean centrosome separation α angle (±s.d.) for control (158.5±14.0°, *n*=30), *ensc* (119.4±26.0°, *n*=21), Ensc-GFP (157.9±14.9°, *n*=19), MBD-GFP (118.6±21.8°, *n*=12) and KBD-GFP (151.3 ±22.6°, *n*=23) NBs. (H) Representation of the α angle distributions of the NBs shown in G. (I) Box plot showing the mean mitotic spindle length (±s.d.) for control (10.9 ±0.7 µm, *n*=24), *ensc* (9.4±0.8 µm, *n*=18), Ensc-GFP (10.5±0.4 µm, *n*=13), MBD-GFP (9.2±0.6 µm, *n*=12) and KBD-GFP (9.3 ±0.8 µm, *n*=22) NBs. ****P<0.0001 (Wilcoxon test); ns, not significant.

monitored the ability of our different Ensconsin variants to restore this process (Palacios and St Johnston, 2002; Serbus et al., 2005; Sung et al., 2008) (Fig. 3E,F). We found, as described previously (Sung et al., 2008), that *ensc* oocytes (*n*=15) showed no ooplasmic streaming, as did MBD-expressing oocytes (*n*=13, Fig. 3F,G). However, expression of Ensc-GFP (*n*=16) efficiently restored ooplasmic particle velocity (*n*=11 oocytes, 123 nm/sec, Fig. 3F-G). KBD-GFP expressing oocytes showed a complete absence (*n*=17/23) or a very slow (*n*=6/23) ooplasmic streaming (*n*=6/23 oocytes, 10 nm/s). To summarize, our data show that Ensconsin KBD is able to sustain efficient Staufen targeting during stage 9 of oogenesis but it but fails to promote ooplasmic streaming and consequently the next step of Staufen polarization during stage 10B.

The Ensconsin KBD promotes minimal recruitment of Kinesin-1 on the oocyte MT network

Kinesin-1 can bind to Ensconsin, and the correct targeting/loading of this motor on MTs is essential for Kinesin-1 function (Metzger et al., 2012). We confirmed, as described previously (Sung et al., 2008), that endogenous Ensconsin is located in the oocyte egg chamber during early stages of oogenesis and also colocalized with the MT cytoskeleton at stage 9 and 10B (Fig. S4C). We decided to examine the localization of Kinesin-1 in oocytes at stage 9 and 10B, the two developmental stages that require Kinesin-1 for direct transport of Staufen particles to the posterior cortex, and for ooplasmic streaming, respectively. The microtubule network of the egg chamber was challenging to detect because of the high

Development (2019) 146, dev171579. doi:10.1242/dev.171579

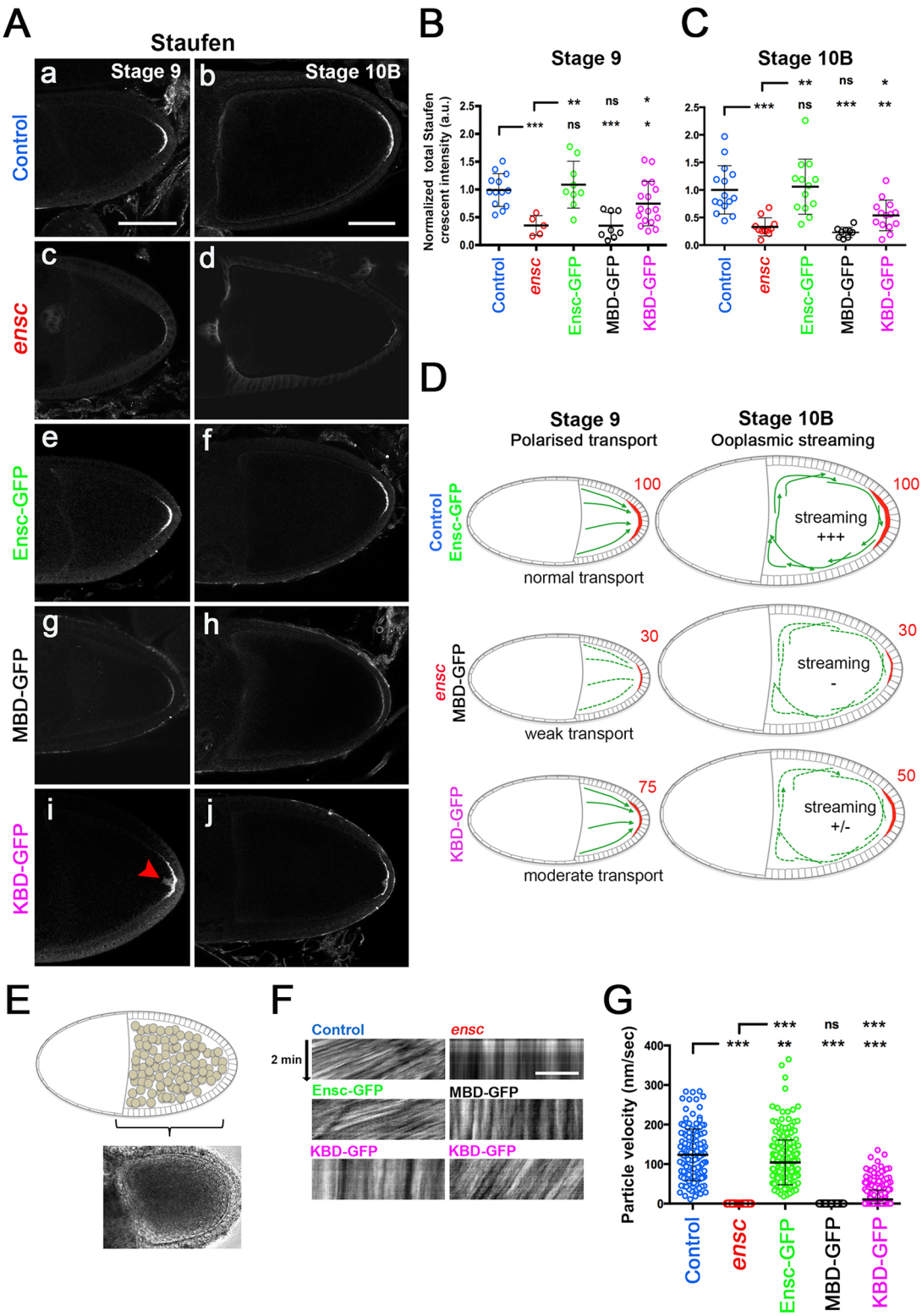

Fig. 3. See next page for legend.

background caused by the presence of free tubulin dimers. Thus, to visualize the microtubule network, as well as MT-associated Kinesin-1 inside the egg chamber, it was necessary to permeabilize the oocyte for 1 h in a MT stabilizing buffer before methanol fixation (Januschke et al., 2006). In control stage 9 oocytes, KHC appeared to be located on the polarized MT network, but the majority of KHC was located at the posterior pole (Fig. 4A, top). In *ensc* and MBD oocytes (Fig. 4A, second and fourth panels from top), this localization pattern was completely impaired. Interestingly, KHC total protein levels were comparable with control extracts in *ensc* mutants, when analysed by western blot, suggesting that the ability of KHC to bind MTs was impaired

Development (2019) 146, dev171579. doi:10.1242/dev.171579

Fig. 3. The Kinesin-binding domain of Ensconsin is not sufficient to restore the Staufen localization in the oocyte egg chamber and fast oocyte streaming. (A) Stage 9 control (a), *ensc* (c) and *ensc* mutant fly oocytes expressing full-length Ensconsin-GFP (e), MBD-GFP (g) or KBD-GFP (i) were stained for Staufen. Stage 10B oocytes from the same five genotypes were stained for Staufen (b,d,f,h,j). The red arrowhead in i indicates defective Staufen localization. (B) Box plot showing the quantification of Staufen crescent intensity (±s.d.) during stage 9. Wild type (1±0.29, *n*=13), *ensc* (0.35 ±0.18, *n*=5), Ensc-GFP (1.08±0.42, *n*=9), MBD (0.35±0.24, *n*=8) and *ensc*; KBD (0.74±0.40, *n*=17). (C) Box plot showing the quantification of Staufen crescent intensity (±s.d.) at stage 10B. Wild type (1.0±0.44, *n*=15), *ensc* (0.33 ±0.16, *n*=11), Ensc-GFP (1.06±0.50, *n*=13), MBD (0.23±0.09, *n*=9) and KBD (0.54±0.28, *n*=14). (D) Schematic view of Staufen transport to the posterior cortex during stages 9 (left) and 10B (right). The Staufen crescent is displayed in red. The microtubule network (in green) is polarized at stage 9 and the arrows indicate the direction of the MT plus-ends. Dotted green lines indicate altered Kinesin-1 transport. The Kinesin-1-mediated polarized transport of Staufen to the posterior cortex is strongly diminished in MBD and *ensc* oocytes but is fully rescued by expression of Ensc-GFP. Expression of KBD is able to rescue 75% of Staufen targeting to the posterior cortex. During stage 10B (top right), a complete reorganization of the MT network occurs. Kinesin-1-mediated MT sliding leads to cytoplasmic mixing of the ooplasm, a process that also contributes to Staufen targeting. Staufen crescent formation is fully rescued by Ensc-GFP and moderately impaired in KBD oocytes, while *ensc* and MBD oocytes display a weak Staufen crescent. (E) Scheme of an oocyte (left) and phase-contrast image of a control oocyte egg chamber (right) where particles are visible. (F) Kymographs showing the displacement of particles from different ooplasms for 2 min. Scale bar: 10 µm. The genotype is indicated at the top of each image. Control (*n*=11, top left panel) and Ensc-GFP-expressing (*n*=16, middle left panel) oocytes show similar particle velocities. *ensc* oocytes (*n*=15, top right panel) and MBD-GFP oocytes (*n*=13, middle right panel) do not show any ooplasmic streaming. KBD (*n*=23) oocytes show either absent (17/23, bottom left panel) or slower ooplasmic streaming (6/23, bottom right panel). (G) Scatter dot plot showing the mean particle velocities (±s.d.) of control (*n*=146, 123±65 nm/s), Ensc-GFP (104±56 nm/s, *n*=243), KBD-GFP (*n*=395, 10±23 nm/sec), MBD-GFP (0 nm/sec, *n*=195) or *ensc* (0 nm/sec, *n*=225) ooplasms. **P*<0.01, ***P*<0.001, ****P*<0.0001, Wilcoxon test. ns, not significant.

following loss of Ensconsin but not KHC stability (Fig. 4A-C and Fig. S3A, right panels). In addition and similarly to brain tissues, Ensconsin protein levels, as well as its ability to bind oocyte MTs, was Kinesin-1 independent (Fig. S3A, left panel, Fig. S3B). Expression of Ensc-GFP completely rescued the correct localization of KHC localization to the posterior pole and on the MT network (Fig. 4A, third panels). Interestingly, at the corresponding stage 9, KHC was present on the MT network and 50% of the pool of KHC appeared to be targeted to the posterior cortex in KBD-GFP oocytes (Fig. 4A, bottom panels Fig. 4B).

In wild-type stage 10B oocytes (*n*=10), Kinesin-1 heavy chain (KHC) was strongly bound to the internal oocyte MT network used for the process of oocyte streaming, similar to previous observations (Januschke et al., 2006) (Fig. 4C, top panels). On the other hand, KHC localization was absent on the MT network of *ensc* oocytes (*n*=7, Fig. 4, second panels from top). This localization was fully restored by the expression of Ensc-GFP (*n*=15, Fig. 4, third panels from top), but not by MBD-GFP (*n*=13 Fig. 4, fourth panels from top). In KBD-GFP-expressing oocytes (*n*=9), the MT network showed a very weak presence of Kinesin-1 (Fig. 4, bottom panels). In most cases, KHC appeared to aggregate around the MT network of these KBD oocytes rather to colocalize with MT bundles (Fig. 4, purple arrows). Altogether, these results suggest that KBD is sufficient to fully rescue centrosome-separation defects in brain NBs (Fig. 2) and to recruit Kinesin-1 in stage 9 but not in stage 10B oocytes. Interestingly, and similar to previous observations, the cytoplasmic arrays of MT bundles in stage 10B oocytes was severely disrupted following *khc* RNAi (Fig. S3B; Lu et al., 2016; Serbus et al., 2005). This was also the case when KHC was not targeted to the MTs by Ensconsin in stage 10B oocytes (Fig. 4C, in *ensc*, MBD and KBD oocytes). To conclude, the presence of Kinesin-1 and also its MT targeting by Ensconsin are required to promote MT bundling and organization, and ultimately oocyte streaming during stage 10B of oogenesis.

The Ensconsin KBD recruits Kinesin-1 to MTs *in vitro*

To assess whether the KBD recruits Kinesin-1 to MTs directly, we used an *in vitro* approach with purified components (Fig. 5B). We performed a co-sedimentation assay with purified proteins and taxol-stabilized microtubules to analyse the effect of KBD on a truncated *Drosophila* Kinesin-1 protein (K560) recruitment in an excess of MTs (Monroy et al., 2018). Interestingly, under our conditions, we found an enrichment of K560 in the MT pellet in the presence, compared with the absence, of KBD (75.1 ±7.1 versus 46.6±3.9% of K560 in the MT pellet in the presence versus the absence of KBD, respectively; *n*=3; *P*=0.0037). In addition, we found that KBD was apparent in the MT pellet only in the presence of K560, but not in its absence (59.7±10.6 versus 2.0 ±1.7% of KBD in the MT pellet in the presence versus the absence of K560, respectively; *n*=3; *P*=0.0007), suggesting these two proteins form a complex that exhibits a higher affinity for MTs. Altogether, our data indicate that KBD is able to recruit enough Kinesin-1 to MTs both *in vitro* and *in vivo*. This recruitment is sufficient to rescue centrosome separation defects in neuroblast, but not to correct transport in oocyte, suggesting that the need for Kinesin-1 recruitment to microtubules depends on the cellular context.

DISCUSSION

Full-length Ensconsin is required for maintaining mitotic spindle size

Ensconsin was first discovered two decades ago and was originally purified from microtubule pellets isolated from epithelial cells (Bulinski and Bossler, 1994). Preliminary overexpression experiments did not reveal modified microtubule dynamics in human interphase cells, and *ensc* mutant *Drosophila* oocytes have normal MT cytoskeletons (Faire et al., 1999). However, changes in Ensc levels affect spindle morphogenesis in fly neural stem cells and in human cultured cells, preventing spindle defects (Bulinski et al., 2001; Gallaud et al., 2014; McHedlishvili et al., 2018). Fly *ensc* mutant NBs display short spindles and have reduced MT polymerization speeds. In addition, Ensconsin strongly stimulates MT polymerization *in vitro*, and its overexpression increases spindle length (Fig. S1). Rescue experiments indicate that neither the MBD-GFP nor KBD-GFP fusion protein is able to restore spindle length, even when expressed at similar levels to full-length Ensconsin-GFP, which efficiently rescues that phenotype. This reveals that, although it has a functional MT-binding sequence, the MBD is not able to stimulate MT polymerization on its own *in vivo*. Further studies at the molecular level will be needed to investigate how the MBD and KBD domains cooperate to stimulate MT polymerization.

Mechanisms of Ensconsin stimulation of Kinesin-1 recruitment to MTs

Several studies have shown a functional connection between Kinesin-1 and Ensconsin. First of all, inhibition of Ensconsin and Kinesin-1 has yielded similar phenotypes in four different studies (Barlan et al., 2013; Gallaud et al., 2014; Metzger et al., 2012; Sung et al., 2008). Second, both proteins colocalize on the internal MT

Development (2019) 146, dev171579. doi:10.1242/dev.171579

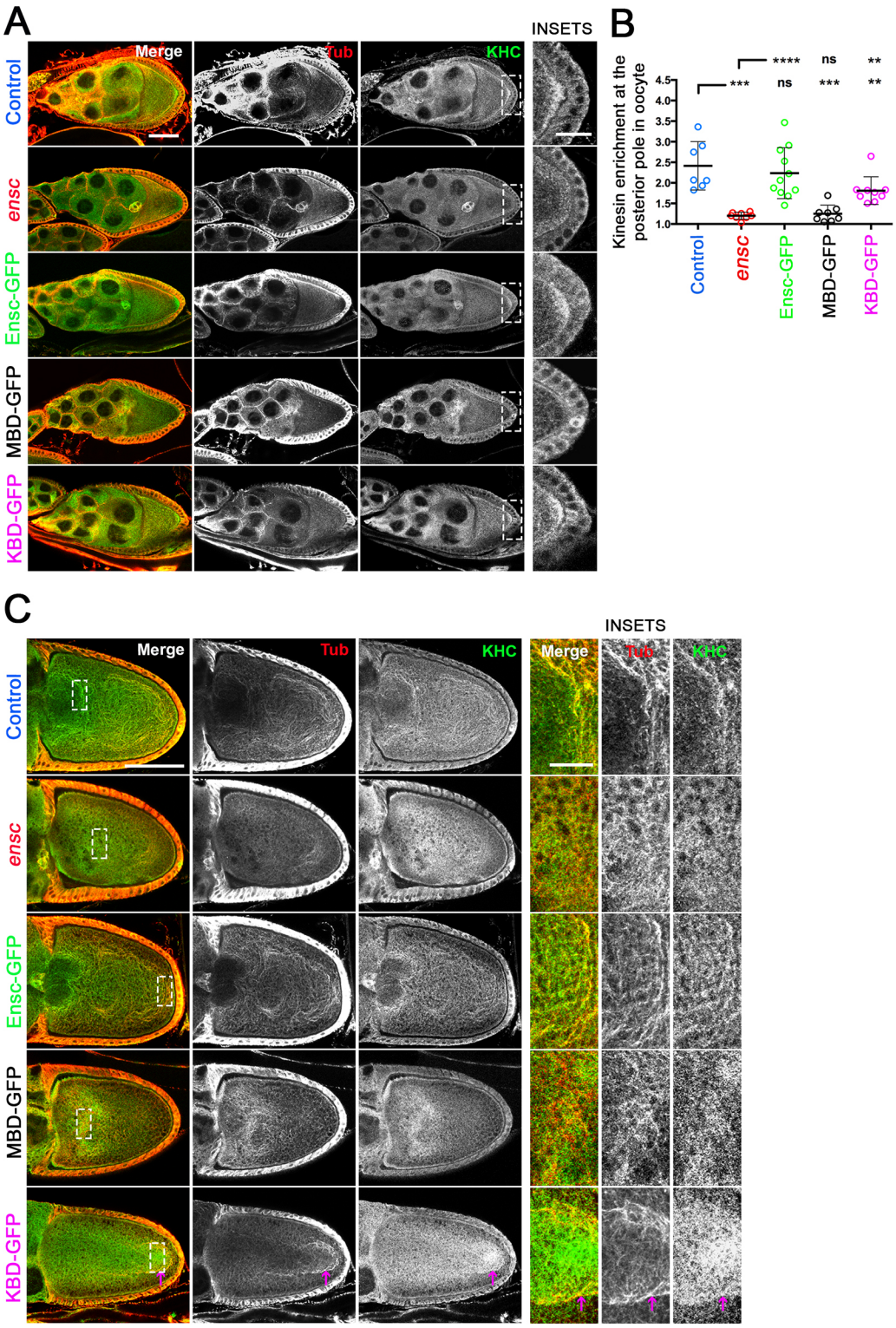

Fig. 4. See next page for legend.

network of *Drosophila* oocyte egg chambers (Sung et al., 2008, this paper). Third, Ensconsin C-terminal domain (KBD) and Kinesin-1 can interact *in vivo* (Hooikaas et al., 2019; Metzger et al., 2012, this study). Based on the current literature, the recruitment model suggests that Ensconsin bound to the MT lattice (via the MBD) serves as a direct recruitment platform for Kinesin-1 (Fig. 5C). This targeting model is supported by Kinesin-1 motor recruitment on MTs, which is lower in *ensc* oocyte extracts and undetectable in intact *ensc* oocytes (Sung et al., 2008, this study, Fig. 4). Furthermore, in Ensconsin and Kinesin-1 knockdown muscle cells, a fusion protein between the Ensc-MBD and the Kinesin-1 motor domain (leading to strong recruitment of the Kinesin motor to the MT network) was able to rescue nuclei spacing, thus strongly supporting the hypothesis that the function of Ensconsin is to deliver

Development (2019) 146, dev171579. doi:10.1242/dev.171579

Fig. 4. The Ensconsin Kinesin-binding domain can promote minimal recruitment of Kinesin-1 on microtubules in oocytes. (A) Stage 9 oocytes of the indicated genotypes were permeabilized for 1 h, fixed and labelled with an anti-tubulin (red in the merge column, monochrome elsewhere) and an anti-Kinesin-1 antibody (green in the merge column, monochrome elsewhere). Scale bar: 50 µm. The right part shows enlarged views of the posterior poles. Scale bar: 20 µm. Wild type and Ensc-GFP show a strong KHC labelling at the posterior side, in contrast to *ensc* or MBD-GFP oocytes, in which KHC is not detectable. KBD-GFP oocytes displayed diminished KHC targeting. (B) Scatter dot plot showing the mean KHC recruitment (a.u.±s.d.) at the posterior side of stage 9 oocytes. Control (n=7, 2.41±0.59), *ensc* (n=8, 1.20±0.59), Ensc-GFP (n=11, 2.24±0.62), MBD-GFP (n=8, 1.25±0.21) and KBD-GFP (n=9, 1.81±0.34 nm/s) ooplasms. **P<0.001, ***P<0.0001, Wilcoxon test. ns, not significant. (C) Stage 10B oocytes of the indicated genotypes were labelled for tubulin (red in the merge column, monochrome elsewhere) and KHC (green in the merge column, monochrome elsewhere). In control oocytes, KHC colocalizes with cytoplasmic bundles of MTs. KHC is lost from the MT network in *ensc* and MBD oocytes and appears as aggregates around the MTs of these oocytes. Ensc-GFP rescues the KHC targeting to MT bundles. Most KBD oocytes (bottom panels) display enrichment of KHC aggregates around cytoplasmic MT bundles, but only few of these bundles exhibit a clear KHC labelling (purple arrow). The right-hand images show enlargements of the outlined areas. Scale bars: 50 µm; 20 µm in enlargements.

Kinesin-1 to MTs (Metzger et al., 2012). Interestingly, this targeting model of Kinesin-1 by MAP7 seems to be required to promote branch formation in rat neurones but is not essential for axon growth (Tymanskyj et al., 2018). Finally, this direct recruitment platform model is supported *in vitro*, as the Kinesin-1 motor is strongly recruited on Ensconsin-labelled MTs (Monroy et al., 2018, Fig. 5). Our study shows that an additional level of regulation comes into play. In fly NBs, Ensconsin and Kinesin-1 are jointly involved in the centrosome separation process (Gallaud et al., 2014). As shown here, this defective centrosomal separation phenotype is completely restored by the simple expression of KBD, independent of microtubules, as we show that KBD does not have the property of binding microtubules. These results confirm the ability of KBD to activate Kinesin-1 in S2 cells and in rat neurones (Barlan et al., 2013; Tymanskyj et al., 2018). This activation is supported by the fact that the KBD/Kinesin-1 motor complex can stimulate the binding of Kinesin-1 to MTs *in vitro* and *in vivo* (Fig. 5B). We believe that this stimulation of the motor binding can occur in solution because we were not able to detect any association of the KBD with MTs either *in vivo* or *in vitro*, as also recently shown by other groups using rat and human Ensconsin (MAP7) (Hooikaas et al., 2019; Tymanskyj et al., 2018). Interestingly, this interaction between Ensconsin and KHC is observed in cell extracts, with or without polymerized microtubules (this work). Intra-molecular auto-inhibition has already been documented through interaction between the motor domain and the tail domain of KHC (Verhey et al., 2011). However, the interaction domain between Ensconsin and Kinesin-1 has been mapped on a different domain on the stem of the *Drosophila* Kinesin-1 stalk, a domain that has not been so far described to exert any self-inhibiting properties on the motor domain. It is possible, as suggested by other groups, that this self-inhibition may be relieved after binding to the KBD of Ensconsin (Hooikaas et al., 2019; Monroy et al., 2018) (see Fig. 5). The relief of inhibition is probably a very transient phenomenon and the disinhibited form of Kinesin-1 has to quickly find a microtubule to land before returning to the auto-inhibited form. This ephemeral interaction between Ensconsin and Kinesin-1 is certainly crucial because Ensconsin is strongly anchored on MTs and a strong interaction with Kinesin-1 would impair subsequent Kinesin-1 movement and probably the jump between crossing MTs, an event proposed to trigger branch formation in neurons (Tymanskyj et al., 2018). Altogether, it will be interesting to examine in the future how these auto-inhibition domains cooperate to regulate Kinesin-1 function in space and time.

On the other hand, this full rescue of Kinesin-1 function is not validated in *ensc* mutant oocytes: the KBD expression only favours a partial localization of Gurken and Staufen. Interestingly, a recent study has demonstrated that Staufen targeting to the posterior pole is a two-step Kinesin-1-dependent process that occurs during stage 9 and 10B of oogenesis. During stage 9, Staufen particles are transported via Kinesin-1 on the polarized MT network, the plus ends of which point towards the posterior pole where these particles are anchored by Myosin V. During stage 10B, the polarized MT network is completely reorganized and Kinesin-1 MT sliding occurs between cytoplasmic bundles and stable cortically anchored MTs. This sliding is responsible for the very fast streaming of Staufen particles that are captured at the posterior pole. These two modes of transport are required for full Staufen delivery (Lu et al., 2018). Interestingly, KBD was able to support 75% of wild-type Kinesin-1-mediated transport of Staufen at stage 9 but was largely inefficient for ooplasm streaming at stage 10B. Our hypothesis is that Kinesin-1 demand during stage 9 is low, suggesting, similar to centrosome separation in NBs, that a weak targeting of Kinesin-1 to the polarized MT arrays by KBD is sufficient for biased transport toward the cortex. Oocyte streaming and MT organization at stage 10B probably requires much more Kinesin-1 targeting to the MT network, which can not be supported by the KBD alone (Serbus et al., 2005).

It is essential to keep in mind, however, that the KBD does not exist in normal cells and corresponds to a domain only present in the full-length Ensconsin protein. However, our rescue experiments have allowed us to reveal a moderate but physiologically relevant property of KBD in targeting Kinesin-1 to the microtubule network *in vivo* and *in vitro*. We believe that MT-bound Ensconsin provides a platform for simultaneously recruiting and transiently stimulating Kinesin-1 binding to MTs (Fig. 5C). The Ensconsin family of proteins can therefore be considered as 'Microtubule-tethered Kinesin-1 activators' (Hooikaas et al., 2019). Remarkably, our data suggest that the model based on high Kinesin-1 targeting of MTs via full-length Ensconsin is not an absolute requirement for development, as KBD flies are viable. This confirms the idea that only a small amount of Kinesin-1 targeting MTs is sufficient to support fly development, at least under laboratory conditions where animals are maintained. However, unlike the flies rescued by the full-length Ensconsin, KBD females remain sterile, perhaps because, in addition to oocyte polarization defects, the *ensc* mutant meiotic spindle is abnormal and does not support correct chromosome segregation (Professor Ohkura, University of Edinburgh, UK, personal communication). In flies, the observed weak targeting of Kinesin-1 on the MT network by KBD is sufficient to sustain Kinesin-1 function in S2 cells, neuroblasts and stage oocytes 9, but not in stage 10B oocytes (Barlan et al., 2013). However, even if the size factor is the first thing that comes to mind when comparing these four cell types, we cannot rule out the hypothesis that the observed recruitment differences are also dependent on other levels of regulation. We cannot exclude, as observed for other MAPs, that Kinesin-1 affinity for the microtubule is also directly related to the presence of particular isoforms of tubulin proteins or under the control of a tubulin code that could vary between cells (Yu et al., 2015). Further studies will be needed to understand how the optimal targeting of Kinesin-1 by Ensconsin on microtubules is achieved according to different cell types.

Development (2019) 146, dev171579. doi:10.1242/dev.171579

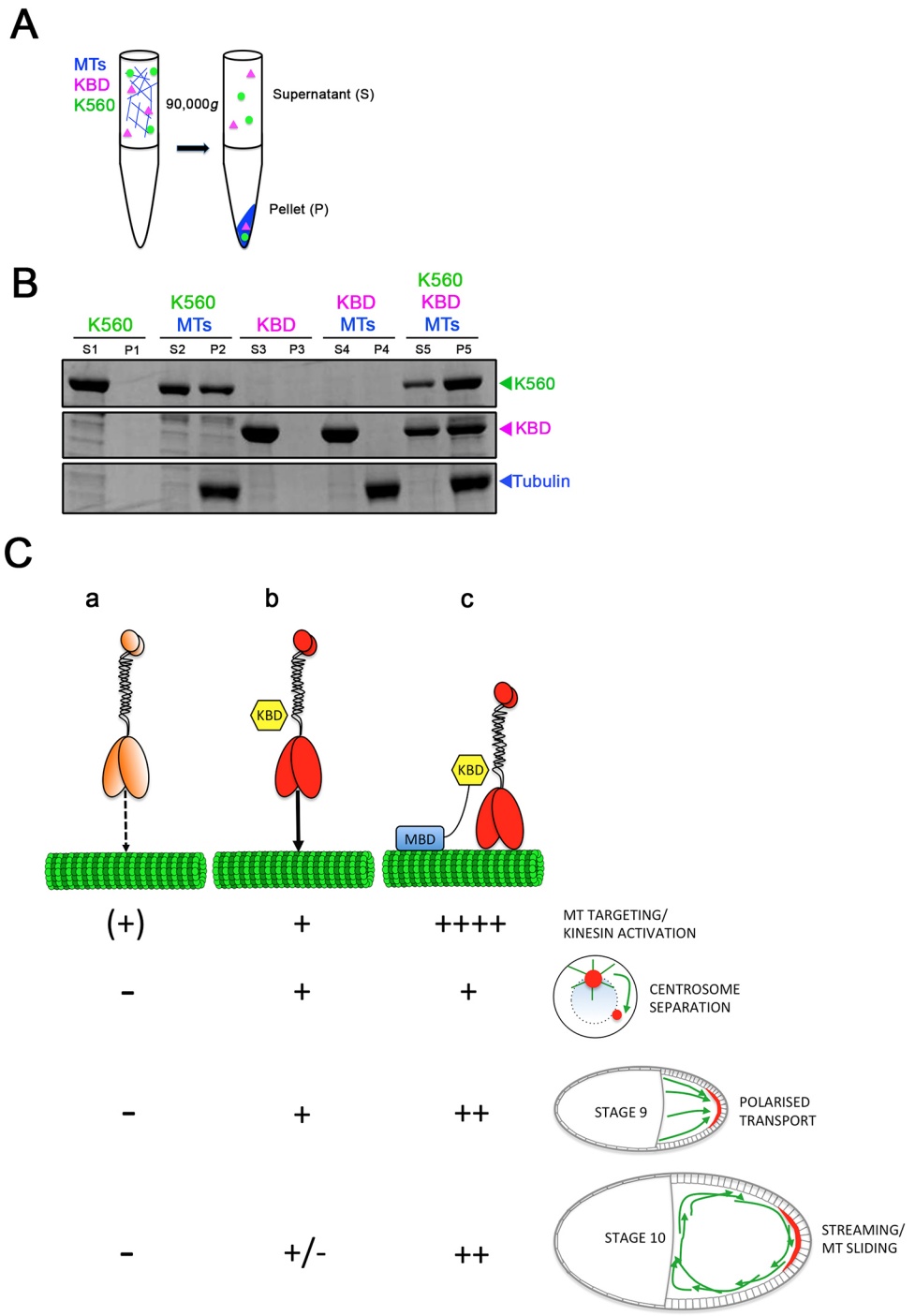

Fig. 5. The Ensconsin Kinesin-binding domain can promote recruitment of K560 to MTs *in vitro*. (A) Scheme of the MT-binding assay. KBD and K560, a truncated KHC protein (amino acids 1-560), were mixed in the presence of polymerized MTs and subjected to centrifugation (see Materials and Methods). MT pellets (P) and supernatants (S) were subsequently analysed by western blot. (B) Coomassie Blue-stained SDS-PAGE gel shows the binding behaviour of 500 nM Ensc-KBD and/or 500 nM K560 in the presence of 2.5 µM taxol-stabilized microtubules. K560 levels increase in the MT pellet in the presence of KBD. The percentages of K560 in the MT pellet are 46.6±3.9% and 75.1 ±7.1% in the absence and presence of Ensconsin KBD, respectively (n=3, P=0.0036). Ensconsin KBD is detected in the MT pellet only in the presence of K560, indicating direct interaction (59.7±10.6% versus 2.0±1.7%, n=3; P=0.0007). (C) Speculative model for dual Kinesin-1 recruitment to MTs and consequences for several Kinesin-1-dependent processes in *Drosophila*. (a) Kinesin-1 (orange) shows intrinsic MT binding, which is weak because of auto-inhibition properties. Flies without Kinesin-1 or Ensconsin cannot separate their centrosomes during interphase, and cannot perform KHC-mediated transport or oocyte streaming during stages 9 and 10B of oogenesis, respectively. (b) Our data suggest that a truncated Kinesin-1 that shows intrinsic binding to MTs can be weakly stimulated after transient interaction with KBD, which may cause a relief of auto-inhibition (red). *In vivo*, this targeting of Kinesin-1 molecules to MTs is sufficient to sustain normal centrosome separation in brain NBs and almost complete Staufen-mediated transport along the polarized MTs network of stage 9 oocytes, but not oocyte streaming in stage 10B of oogenesis. (c) *In vivo*, MT-anchored Ensconsin serves as a platform to simultaneously recruit and stimulate Kinesin-1 targeting to the MTs. This dual activation is essential for efficient oocyte streaming in stage 10B oocytes.

MATERIALS AND METHODS

DNA constructs

Histidine-tagged expression constructs were generated as previously described using: full-length Ensconsin; Ensc-MBD, the N-terminal domain of which contains the microtubule-binding domain, also referred to as EHR1; and Ensc-KBD, the C-terminal domain containing the Kinesin-binding domain, also referred to as EHR2 (Gallaud et al., 2014; Sung et al., 2008). Ensc-MBD and Ensc-KBD were also introduced into the pUWG vector to generate fly expression constructs for the ubiquitous expression of GFP-tagged proteins. Full-length Ensconsin was introduced in the pTWV vector to generate overexpression of a VenusFP-protein under the control of the GAL protein. pUWG and pTWG were purchased from the Drosophila Genomics Resource Center. The *Drosophila* Kinesin-1 expression construct K560 (amino acids 1-560, a gift from R. Vale, University of California, San Franciso, CA, USA) was cloned in frame using Gibson cloning into pET28 vector with a C-terminal mScarlet-strepII cassette (Monroy et al., 2018).

Fly strains

Flies were maintained under standard conditions at 25°C. All studies were performed using *enscΔnull* and *enscΔN ensconsin* mutants (Sung et al., 2008). In contrast with previous studies, western blotting experiments using an antibody raised against the C-terminal region of Ensconsin revealed the *enscΔN allele* is a null allele (Gallaud et al., 2014). *enscΔnull* is also a null allele but the deletion also removes a piece of the neighbouring gene (Sung et al., 2008). All experiments were therefore performed in trans-heterozygous *enscΔnull*/*enscΔN* flies, hereafter referred to as *ensc* flies.

Development (2019) 146, dev171579. doi:10.1242/dev.171579

khc mutant flies carrying amino acid substitutions have been described elsewhere and were provided by A. Guichet (Institut Jacques Monod, Paris, France), B. Saxton (University of California, Santa Cruz, CA, USA) and A. Ephrussi (European Molecular Biology Laboratory, Heidelberg, Germany) (Djagaeva et al., 2012). We have shown in a previous study that the combination of khc^{27} (null allele) and khc^{63} (hypomorphic allele) used in this study exhibits severe centrosome separation defects before mitosis (Gallaud et al., 2014).

Transgenic flies were obtained from BestGene following P-element-mediated transformation with the pTWV vector containing full-length Ensconsin, or the pUWG vector containing the FL-Ensc, Ensc-KBD or Ensc-MBD sequences. The Ensc-GFP and the Ensc-KBD-GFP but not the Ensc-MBD-GFP transgenic proteins rescued the semi-lethality of the *enscΔnull* and *enscΔN* mutants, and the trans-heterozygous *ensc* flies. Unless specified, Ensc-GFP, KBD-GFP and MBD-GFP refer to transgenic animals expressing the corresponding GFP-tagged proteins in an *ensc* background. RFP-tubulin-expressing flies were given to us by Renata Basto (Institut Curie, Paris, France). The 69B-GAL4 strain is from Bloomington Stock Center and was used to drive overexpression of Ensconsin-Venus in brain tissues (Ensc OE). All other GFP and RFP fusion proteins were ubiquitously produced under the control of the polyubiquitin promoter.

Antibodies and western blotting

The monoclonal YL1/2 rat anti-detyrosinated tubulin antibody (1:200) and the mouse monoclonal and rabbit polyclonal anti-phosphorylated histone H3 (Ser10) antibodies (1:500) were obtained from Millipore. The mouse anti-GFP monoclonal antibody (1:1000) was obtained from Roche. The rabbit and rabbit anti-actin (1:4000) polyclonal antibodies, and the anti-Staufen antibody (1:1000) are from Santa Cruz Biotechnology. The rabbit polyclonal anti-KHC antibody (1:2000) was obtained from Cytoskeleton. The mouse monoclonal anti-Gurken antibody (1:200) was from the Developmental Studies Hybridoma Bank. The production of the anti-Ensconsin antibody has been previously described, and the antibody was raised against the Kinesin-binding domain (Gallaud et al., 2014). The goat peroxidase-conjugated secondary antibodies (1:5000) were obtained from Jackson ImmunoResearch and donkey Alexa Fluor-conjugated secondary antibodies (1:1000) came from Life Technologies. For western blotting, ECL reagent was purchased from Thermo Fisher Scientific.

Live microscopy

Brains expressing the various GFP- or RFP-tagged proteins were dissected in Schneider's *Drosophila* medium containing 10% FCS. Isolated brains were loaded and mounted on stainless steel slides. The preparations were sealed with mineral oil (Sigma) as previously described (Gallaud et al., 2014). Images were acquired using a spinning-disk system mounted on an Eclipse Ti inverted microscope (Nikon) equipped with a 60×1.4 NA objective at 25°C. *Z*-series were acquired every 30 or 60 s with a Photometrics CCD camera (CoolSNAP HQ2) and an sCMOS ORCA-Flash4.0 (Hamamatsu) controlled using MetaMorph acquisition software (version X). Images were processed using ImageJ software and are presented as maximum-intensity projections. Embryos were collected on agar plates supplemented with grape juice at 25°C. They were dechorionated by hand using double-sided adhesive tape, then mounted in mineral oil as previously described (Giet et al., 2002). *Z*-series images were acquired every 30 s using either a spinning disk system or a Leica SP5 confocal microscope equipped with a 40×1.3 NA objective at 25°C. For ooplasmic streaming analyses, young females were mated with males and fattened with dried yeast for 3 (controls, KBD-GFP or Ensc-GFP) to 5 days (MBD-GFP or *ensc*), anesthetized and their ovaries removed from the abdomen with fine forceps. Stage 10B oocytes were isolated with two 27-gauge syringes needles in Halocarbon oil (Sigma), mounted and observed by light microscopy using a DMRXA2 microscope (Leica). Velocity analyses of the particles were performed as described in two separate studies (Lu et al., 2016; Serbus et al., 2005) except that three kymographs were obtained for each oocyte along active flows and five particles (15 per oocyte) were analysed for each kymograph using the Multikymograph plug-in for Fiji.

Observation of Ensc-GFP, KBD-GFP and MBD-GFP was performed in young oocytes also expressing RFP-tubulin after fast dissection of the ovary in PBS and direct observation of the live tissues under the microscope.

The analysis of centrosome separation in larval brain neuroblasts was performed as described previously (Gallaud et al., 2014). The mother and daughter centrosomes were easily distinguished by their different microtubule nucleation potentials shortly before mitosis (Rebollo et al., 2007). Briefly, the separation angle between the two centrosomes was determined 30 s before NEBD, by drawing a line crossing the mother centrosome, the nucleus centre and the daughter centrosome, and calculated using the angle measurement tool for Fiji. In control neuroblasts, most centrosomes are fully separated before mitosis and this angle is between 120 and 180°.

Immunofluorescence in fly oocytes

Oocytes were collected from 2-day-old females. To visualize the MT network, endogenous Ensconsin, KHC and Ensc-GFP fusion protein, oocytes were permeabilized at 25°C in 1% Triton X100 in BRB80 buffer [80 mM K-PIPES, 1 mM $MgCl_2$, 1 mM EGTA (pH 6.8)] and fixed with −20°C methanol as described previously (Januschke et al., 2006).

For Staufen and Gurken localization, four to eight ovaries were fixed with PBS buffer containing 4% paraformaldehyde and 0.1% Triton X-100, washed three times for 5 min in PBST (PBS+0.1% Triton X-100) and blocked on PBST containing 1% BSA. Incubation with the primary antibodies was performed overnight at room temperature in BBT (PBS containing 0.1% BSA and 0.1% Tween 20). The ovaries were then briefly washed three times and three times for 30 min each in BBT. The Alexa-conjugated secondary antibody was incubated for 2 h at room temperature. The ovaries were then washed three times for 15 min each time in PBST, dissected and mounted in ProLong Gold (Invitrogen).

Immunofluorescence in fly brain by methanol fixation

Wild-type or khc^{27}/khc^{63} larval brains were dissected in Schneider media supplemented with 10% of decomplemented foetal calf serum (Invitrogen). When five brains were dissected, they were transferred in 20 µl of Schneider media. The brains were then gently aspired with the tip of a Pasteur pipette and immediately transferred in 1 ml of methanol pre-chilled at −20°C. The tubes were then transferred for 15 min at −20°C. After fixation, the methanol was discarded and the tissues were washed three times for 5 min in PBST with gentle agitation at room temperature, blocked with PBSTB (PBST supplemented with 1% BSA) and incubated with primary antibodies overnight at 4°C in PBSTB. The brains were then washed three times for 15 min in PBST and incubated with secondary antibodies for 2 h at room temperature in PBSTB. After three washes in PBST, the tissues were mounted in ProLong Gold (Invitrogen).

Protein expression and purification

Tubulin was isolated from porcine brain using the high-molarity PIPES procedure as previously described (Castoldi and Popov, 2003). For bacterial expression, K560-mScarlet, BL21-RIPL cells were grown at 37°C until ∼0.6 OD and protein expression was induced using 0.1 mM IPTG. Cells were grown overnight at 18°C, harvested and frozen. Cell pellets were resuspended in lysis buffer [50 mM Tris (pH 8), 150 mM K-acetate, 2 mM Mg-acetate, 1 mM EGTA, 10% glycerol] with protease inhibitor cocktail (Roche), 1 mM DTT, 1 mM PMSF and DNAseI. Cells were then passed through an Emulsiflex press and cleared by centrifugation at 23,000 ***g*** for 20 min. Clarified lysate was passed over a column with Streptactin Superflow resin (Qiagen). After incubation, the column was washed with four column volumes of lysis buffer, then bound proteins were eluted with 3 mM desthiobiotin (Sigma) in lysis buffer. Eluted proteins were concentrated on Amicon concentrators and passed through a superose-6 (GE Healthcare) gel-filtration column in lysis buffer using a Bio-Rad NGC system. Peak fractions were collected, concentrated and flash frozen in LN_2. Protein concentration was determined by measuring the absorbance of the fluorescent protein tag and calculated using the molar extinction coefficient of the tag. The resulting preparations were analysed by SDS-PAGE. Bacterial expression of hexa histidine-tagged KBD was performed as described previously (Gallaud et al., 2014) except that the protein was

Development (2019) 146, dev171579. doi:10.1242/dev.171579

dialysed overnight against PBS, and concentrated using Amicon Ultra-4 Centrifugal filters (Millipore). The proteins were stored at −80°C.

Immunoprecipitation experiments

Thirty females expressing either MBD, KBD or full-length GFP-tagged Ensconsin were lysed using a French press in 500 µl of lysis buffer [LB 10 mM Tris, 150 mM NaCl, 0.5 mM EDTA (pH 7.4)] supplemented with 0.05% NP-40, 1 mM DTT containing 5× proteases inhibitors (Roche). The extracts were centrifuged at 10,000 ***g*** for 30 min at 4°C and the supernatants were incubated with 10 µl of GFP-Trap beads (Chromotek) for 1 h on a rotating wheel. The beads were washed three times with LB and the bound proteins were analysed by western blotting with anti-GFP and anti-KHC antibodies.

Microtubule co-sedimentation assay

Microtubules were prepared by polymerizing 25 mg/ml of porcine tubulin in assembly buffer (BRB80 buffer supplemented with 1 mM GTP, 1 mM DTT) at 37°C for 15 min, then a final concentration of 20 µM taxol was added to the solution, which was incubated at 37°C for an additional 15 min. Microtubules were pelleted over a 25% sucrose cushion at 100,000 ***g*** at 25°C for 10 min, then resuspended in BRB80 buffer with 1 mM DTT and 10 µM taxol. Binding reactions were carried out by mixing 500 nM of sfGFP-Ensconsin-KBD and/or 500 nM mScarlet-K560 (that had been pre-centrifuged at 100,000 ***g***) with 2.5 µM of microtubules in assay buffer [50 mM Tris (pH 8), 50 mM potassium acetate, 2 mM magnesium acetate, 1 mM EGTA, 10% glycerol and supplemented with 1 mM DTT, 10 µM taxol] and incubated at 25°C for 10 min. The mixtures were then pelleted at 90,000 ***g*** at 25°C for 10 min. Supernatant and pellet fractions were recovered, resuspended in sample buffer, run on an SDS-PAGE gel and then stained with Coomassie Blue. Protein band intensities were quantified using ImageJ.

Statistical analysis

All statistical tests were performed using the Wilcoxon test or a two-tailed Student's *t*-test for MT co-pelleting assays.

Acknowledgements

We thank R. Basto for the kind gift of RFP-tubulin-expressing flies. We thank Kahina Sadaouli for the preliminary functional analyses of Ensconsin domains during oocyte development. We thank the Microscopy Rennes Imaging Center for the microscopy facilities. We thank Christelle Benaud, Romain Gibeaux and Denis Chrétien for critical reading and helpful comments on the manuscript.

Competing interests

The authors declare no competing or financial interests.

Author contributions

Conceptualization: M.M., B.Y.M., E.G., R.C., A.G., K.M.O.-M., R.G.; Methodology: M.M., B.Y.M., E.G., R.C., A.P., A.G., K.M.O.-M., R.G.; Validation: M.M., B.Y.M., A.P., K.M.O.-M., R.G.; Formal analysis: M.M., B.Y.M., E.G., R.C., K.M.O.-M., R.G.; Investigation: M.M., B.Y.M., E.G., R.C., A.P., A.G., K.M.O.-M., R.G.; Writing - original draft: M.M., R.G.; Writing - review & editing: M.M., B.Y.M., E.G., R.C., L.R.-P., A.G., K.M.O.-M., R.G.; Visualization: M.M., B.Y.M., E.G., R.C., A.G., K.M.O.-M., R.G.; Supervision: L.R.-P., A.G., K.M.O.-M., R.G.; Project administration: R.G.; Funding acquisition: K.M.O.-M., R.G.

Funding

This work was funded by the Ligue Contre le Cancer and the Fondation ARC pour la Recherche sur le Cancer. M.M. is a doctoral fellow of the Région Bretagne and the Ligue Contre le Cancer. E.G. was a doctoral fellow of the Région Bretagne. R.G. is supported by the Centre National de la Recherche Scientifique, the University of Rennes, The Ligue Contre le Cancer and the Fondation ARC pour la Recherche sur le Cancer. A.G. was supported by the Centre National de la Recherche Scientifique and by the Fondation ARC pour la recherche sur le cancer (PJA 20161204931). K.M.O.-M. is supported by the National Institutes of Health (R00HD080981), the March of Dimes Foundation and the Simons Foundation. Deposited in PMC for release after 12 months.

Supplementary information

Supplementary information available online at
http://dev.biologists.org/lookup/doi/10.1242/dev.171579.supplemental

References

Barlan, K. and Gelfand, V. I. (2017). Microtubule-based transport and the distribution, tethering, and organization of organelles. *Cold Spring Harb. Perspect Biol.* **9**, a025817. doi:10.1101/cshperspect.a025817

Barlan, K., Lu, W. and Gelfand, V. I. (2013). The microtubule-binding protein ensconsin is an essential cofactor of kinesin-1. *Curr. Biol.* **23**, 317-322. doi:10.1016/j.cub.2013.01.008

Brendza, R. P., Serbus, L. R., Duffy, J. B. and Saxton, W. M. (2000). A function for kinesin I in the posterior transport of oskar mRNA and Staufen protein. *Science* **289**, 2120-2122. doi:10.1126/science.289.5487.2120

Brendza, R. P., Serbus, L. R., Saxton, W. M. and Duffy, J. B. (2002). Posterior localization of dynein and dorsal-ventral axis formation depend on kinesin in Drosophila oocytes. *Curr. Biol.* **12**, 1541-1545. doi:10.1016/S0960-9822(02)01108-9

Bulinski, J. C. and Bossler, A. (1994). Purification and characterization of ensconsin, a novel microtubule stabilizing protein. *J. Cell Sci.* **107**, 2839-2849.

Bulinski, J. C., Odde, D. J., Howell, B. J., Salmon, T. D. and Waterman-Storer, C. M. (2001). Rapid dynamics of the microtubule binding of ensconsin in vivo. *J. Cell Sci.* **114**, 3885-3897.

Castoldi, M. and Popov, A. V. (2003). Purification of brain tubulin through two cycles of polymerization-depolymerization in a high-molarity buffer. *Protein Expr. Purif.* **32**, 83-88. doi:10.1016/S1046-5928(03)00218-3

Conduit, P. T. and Raff, J. W. (2010). Cnn dynamics drive centrosome size asymmetry to ensure daughter centriole retention in Drosophila neuroblasts. *Curr. Biol.* **20**, 2187-2192. doi:10.1016/j.cub.2010.11.055

Djagaeva, I., Rose, D. J., Lim, A., Venter, C. E., Brendza, K. M., Moua, P. and Saxton, W. M. (2012). Three routes to suppression of the neurodegenerative phenotypes caused by kinesin heavy chain mutations. *Genetics* **192**, 173-183. doi:10.1534/genetics.112.140798

Duncan, J. E. and Warrior, R. (2002). The cytoplasmic dynein and kinesin motors have interdependent roles in patterning the Drosophila oocyte. *Curr. Biol.* **12**, 1982-1991. doi:10.1016/S0960-9822(02)01303-9

Faire, K., Waterman-Storer, C. M., Gruber, D., Masson, D., Salmon, E. D. and Bulinski, J. C. (1999). E-MAP-115 (ensconsin) associates dynamically with microtubules in vivo and is not a physiological modulator of microtubule dynamics. *J. Cell Sci.* **112**, 4243-4255.

Ferrandon, D., Elphick, L., Nüsslein-Volhard, C. and St Johnston, D. (1994). Staufen protein associates with the 3'UTR of bicoid mRNA to form particles that move in a microtubule-dependent manner. *Cell* **79**, 1221-1232. doi:10.1016/0092-8674(94)90013-2

Gallaud, E., Caous, R., Pascal, A., Bazile, F., Gagné, J.-P., Huet, S., Poirier, G. G., Chrétien, D., Richard-Parpaillon, L. and Giet, R. (2014). Ensconsin/Map7 promotes microtubule growth and centrosome separation in Drosophila neural stem cells. *J. Cell Biol.* **204**, 1111-1121. doi:10.1083/jcb.201311094

Giet, R., McLean, D., Descamps, S., Lee, M. J., Raff, J. W., Prigent, C. and Glover, D. M. (2002). Drosophila Aurora A kinase is required to localize D-TACC to centrosomes and to regulate astral microtubules. *J. Cell Biol.* **156**, 437-451. doi:10.1083/jcb.200108135

Heald, R. and Khodjakov, A. (2015). Thirty years of search and capture: The complex simplicity of mitotic spindle assembly. *J. Cell Biol.* **211**, 1103-1111. doi:10.1083/jcb.201510015

Hooikaas, J., Martin, M., Kuijntjes, G., Peeters, C., Katrukha, E., Ferrari, L., Stucchi, R., Verhagen, D., van Riel, W., Maarten Altelaar, A., (2019). MAP7 family proteins are microtubule-tethered allosteric activators of kinesin-1. *J. Cell Biol.* **218**, 1298-1318. doi:10.1083/jcb.201808065

Januschke, J., Gervais, L., Dass, S., Kaltschmidt, J. A., Lopez-Schier, H., St Johnston, D., Brand, A. H., Roth, S. and Guichet, A. (2002). Polar transport in the Drosophila oocyte requires Dynein and Kinesin I cooperation. *Curr. Biol.* **12**, 1971-1981. doi:10.1016/S0960-9822(02)01302-7

Januschke, J., Gervais, L., Gillet, L., Keryer, G., Bornens, M. and Guichet, A. (2006). The centrosome-nucleus complex and microtubule organization in the Drosophila oocyte. *Development* **133**, 129-139. doi:10.1242/dev.02179

Januschke, J., Llamazares, S., Reina, J. and Gonzalez, C. (2011). Drosophila neuroblasts retain the daughter centrosome. *Nat. Commun.* **2**, 243. doi:10.1038/ncomms1245

Lu, W., Winding, M., Lakonishok, M., Wildonger, J. and Gelfand, V. I. (2016). Microtubule-microtubule sliding by kinesin-1 is essential for normal cytoplasmic streaming in Drosophila oocytes. *Proc. Natl. Acad. Sci. USA* **113**, E4995-E5004. doi:10.1073/pnas.1522424113

Lu, W., Lakonishok, M., Serpinskaya, A. S., Kirchenbüechler, D., Ling, S.-C. and Gelfand, V. I. (2018). Ooplasmic flow cooperates with transport and anchorage in Drosophila oocyte posterior determination. *J. Cell Biol.* **217**, 3497-3511. doi:10.1083/jcb.201709174

McHedlishvili, N., Matthews, H. K., Corrigan, A. and Baum, B. (2018). Two-step interphase microtubule disassembly aids spindle morphogenesis. *BMC Biol.* **16**, 14. doi:10.1186/s12915-017-0478-z

Metzger, T., Gache, V., Xu, M., Cadot, B., Folker, E. S., Richardson, B. E., Gomes, E. R. and Baylies, M. K. (2012). MAP and kinesin-dependent nuclear positioning is required for skeletal muscle function. *Nature* **484**, 120-124. doi:10.1038/nature10914

Mitchison, T. and Kirschner, M. (1984). Dynamic instability of microtubule growth. *Nature* **312**, 237-242. doi:10.1038/312237a0

Monroy, B. Y., Sawyer, D. L., Ackermann, B. E., Borden, M. M., Tan, T. C. and Ori-McKenney, K. M. (2018). Competition between microtubule-associated proteins directs motor transport. *Nat. Commun.* **9**, 1487. doi:10.1038/s41467-018-03909-2

Neuman-Silberberg, F. S. and Schupbach, T. (1993). The Drosophila dorsoventral patterning gene gurken produces a dorsally localized RNA and encodes a TGF alpha-like protein. *Cell* **75**, 165-174. doi:10.1016/S0092-8674(05)80093-5

Palacios, I. M. and St Johnston, D. (2002). Kinesin light chain-independent function of the Kinesin heavy chain in cytoplasmic streaming and posterior localisation in the Drosophila oocyte. *Development* **129**, 5473-5485. doi:10.1242/dev.00119

Rebollo, E., Sampaio, P., Januschke, J., Llamazares, S., Varmark, H. and González, C. (2007). Functionally unequal centrosomes drive spindle orientation in asymmetrically dividing Drosophila neural stem cells. *Dev. Cell* **12**, 467-474. doi:10.1016/j.devcel.2007.01.021

Rusan, N. M. and Peifer, M. (2007). A role for a novel centrosome cycle in asymmetric cell division. *J. Cell Biol.* **177**, 13-20. doi:10.1083/jcb.200612140

Serbus, L. R., Cha, B. J., Theurkauf, W. E. and Saxton, W. M. (2005). Dynein and the actin cytoskeleton control kinesin-driven cytoplasmic streaming in Drosophila oocytes. *Development* **132**, 3743-3752. doi:10.1242/dev.01956

St Johnston, D., Beuchle, D. and Nüsslein-Volhard, C. (1991). Staufen, a gene required to localize maternal RNAs in the Drosophila egg. *Cell* **66**, 51-63. doi:10.1016/0092-8674(91)90138-O

Sung, H.-H., Telley, I. A., Papadaki, P., Ephrussi, A., Surrey, T. and Rorth, P. (2008). Drosophila ensconsin promotes productive recruitment of Kinesin-1 to microtubules. *Dev. Cell* **15**, 866-876. doi:10.1016/j.devcel.2008.10.006

Tymanskyj, S. R., Yang, B. H., Verhey, K. J. and Ma, L. (2018). MAP7 regulates axon morphogenesis by recruiting kinesin-1 to microtubules and modulating organelle transport. *Elife* **7**, e36374. doi:10.7554/eLife.36374

Verhey, K. J., Kaul, N. and Soppina, V. (2011). Kinesin assembly and movement in cells. *Annu. Rev. Biophys.* **40**, 267-288. doi:10.1146/annurev-biophys-042910-155310

Walczak, C. E. and Heald, R. (2008). Mechanisms of mitotic spindle assembly and function. *Int. Rev. Cytol.* **265**, 111-158. doi:10.1016/S0074-7696(07)65003-7

Yu, I., Garnham, C. P. and Roll-Mecak, A. (2015). Writing and Reading the Tubulin Code. *J. Biol. Chem.* **290**, 17163-17172. doi:10.1074/jbc.R115.637447

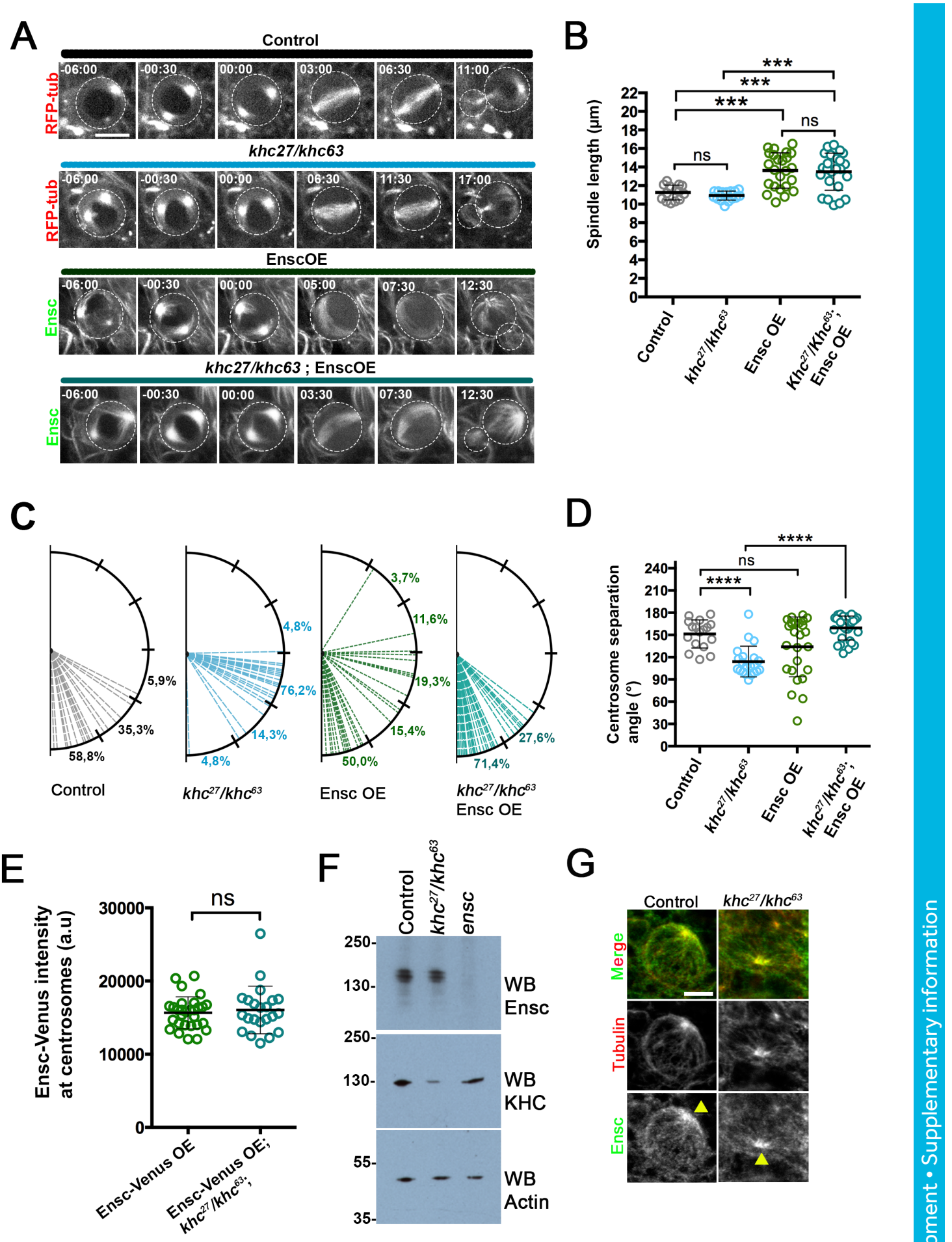
A
Control
RFP-tub
-06:00
-00:30
00:00
03:00
06:30
11:00
khc27/khc63
RFP-tub
-06:00
-00:30
00:00
06:30
11:30
17:00
EnscOE
Ensc
-06:00
-00:30
00:00
05:00
07:30
12:30
khc27/khc63 ; EnscOE
Ensc
-06:00
-00:30
00:00
03:30
07:30
12:30
B
Spindle length (µm)
***
***
***
ns
ns
Control
khc27/khc63
Ensc OE
Khc27/Khc63; Ensc OE
C
5,9%
35,3%
58,8%
Control
4,8%
76,2%
14,3%
4,8%
khc27/khc63
3,7%
11,6%
19,3%
15,4%
50,0%
Ensc OE
27,6%
71,4%
khc27/khc63 Ensc OE
D
Centrosome separation angle (°)
****
ns
****
Control
khc27/khc63
Ensc OE
khc27/khc63; Ensc OE
E
Ensc-Venus intensity at centrosomes (a.u)
ns
Ensc-Venus OE
Ensc-Venus OE; khc27/khc63;
F
Control
khc27/khc63
ensc
WB Ensc
WB KHC
WB Actin
G
Control
khc27/khc63
Merge
Tubulin
Ensc

Figure S1. Overexpression of Ensconsin increases mitotic spindle length in a Kinesin-1-independent manner but efficiently rescues *khc*-dependent centrosome separation defects and in brain NBs.

A) Dividing neuroblasts were imaged in four different genotypes: control, khc^{27}/khc^{63}, Ensconsin-Venus overexpression (Ensc OE) and in khc^{27}/khc^{63}overexpressing Ensconsin (khc^{27}/khc^{63}; Ensc OE). Scale bar:10 μm. Time is min:sec. B) Box plot showing the mean (± s.d.) mitotic spindle length analysis for control (11.3 ± 0.8 μm, *n*=14), khc^{27}/khc^{63} (10.9 ± 0.5 μm, *n*=17), Ensc OE (13.6 ± 1.9 μm, *n*=24), khc^{27}/khc^{63} ; Ensc OE (13.5 ± 2.0 μm, *n*=24) NBs. ***, $P < 0.001$ (Wilcoxon test). C) Analysis of centrosome separation angle (α) at NEBD for the indicated genotypes. D) Box plot showing the mean (± s.d.) centrosome separation angle for control (151.4 ± 19.0°, *n*=17), khc^{27}/khc^{63} (114.1 ± 20.7°, *n*=21), Ensc OE (134.0 ± 40.3°, *n*=26), khc^{27}/khc^{63}; Ensc OE (159.4 ±16.2°, *n*=29) NBs, corresponding to panel C. ****, $P < 0.0001$ (Wilcoxon test). E) Scatter box blot showing the mean value (± s.d.) of Ensc-Venus centrosomal signal (a.u) 30 sec before NEBD in WT (15659±2188, *n*=29) or khc^{27}/khc^{63} (16038±3255, *n*=22). F) Western blot showing Ensconsin, KHC and actin (as a loading control) protein levels in WT, khc^{27}/khc^{63} mutant and *ensc* mutant brain extracts. KHC levels are stable in *ensc* mutants (and vice versa). G) Endogenous Ensconsin localization during interphase in control (left) and in khc^{27}/khc^{63} mutant NBs (right). Tubulin is red in the merge panels and monochrome in the middle panels. Ensconsin is Green in the merge panels and Monochrome in the bottom panels. Scale bar: 5 μm.

Development • Supplementary information

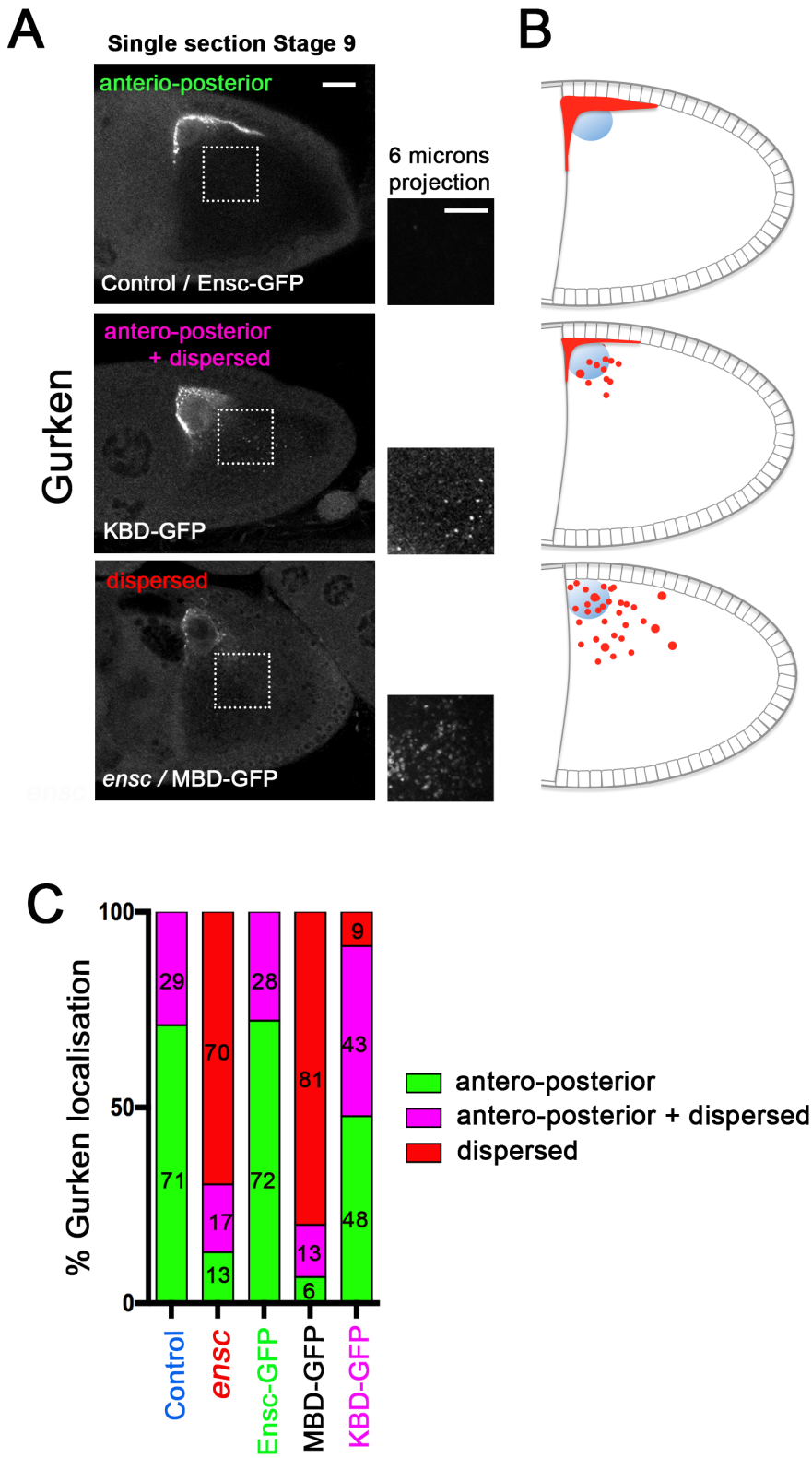

Development • Supplementary information

Figure S2. Gurken localization in oocytes (revoir les numerous avec le texte)

A) Gurken localization patterns at stage 9 in different genetic backgrounds. Gurken is mainly located at the dorsal corner side of the nucleus in both control and Ensc-GFP. Note that it can also appear as tiny dots around the nucleus. In *ensc* and MBD-GFP, Gurken signal was dispersed or appeared as tiny spots around the nucleus (bottom). In KBD-GFP oocytes (middle), some oocytes showed a WT Gurken distribution (11/23), a small portion of the oocytes has a Gurken localization pattern comparable to *ensc* mutant (2/23) and the remaining oocytes displayed an intermediate phenotype with a punctiform distribution at the dorsal side corner region (10/23). B) Schematic diagram of Gurken localization (red) in stage 9 oocytes that summarises a representative oocyte for WT and Ensc-GFP (top), KBD-GFP (middle) and in *ensc* and MBD-GFP backgrounds (bottom). The nucleus is shown as blue sphere. C) Histogram showing the percentage distribution of Gurken localization in stage 9 oocytes for controls (n=14) , *ensc* (*n*=23), MBD-GFP (*n*=15), KBD-GFP (*n*=23) and Ensc-GFP (*n*=18). Numbers in the columns correspond to percentages.

Development • Supplementary information

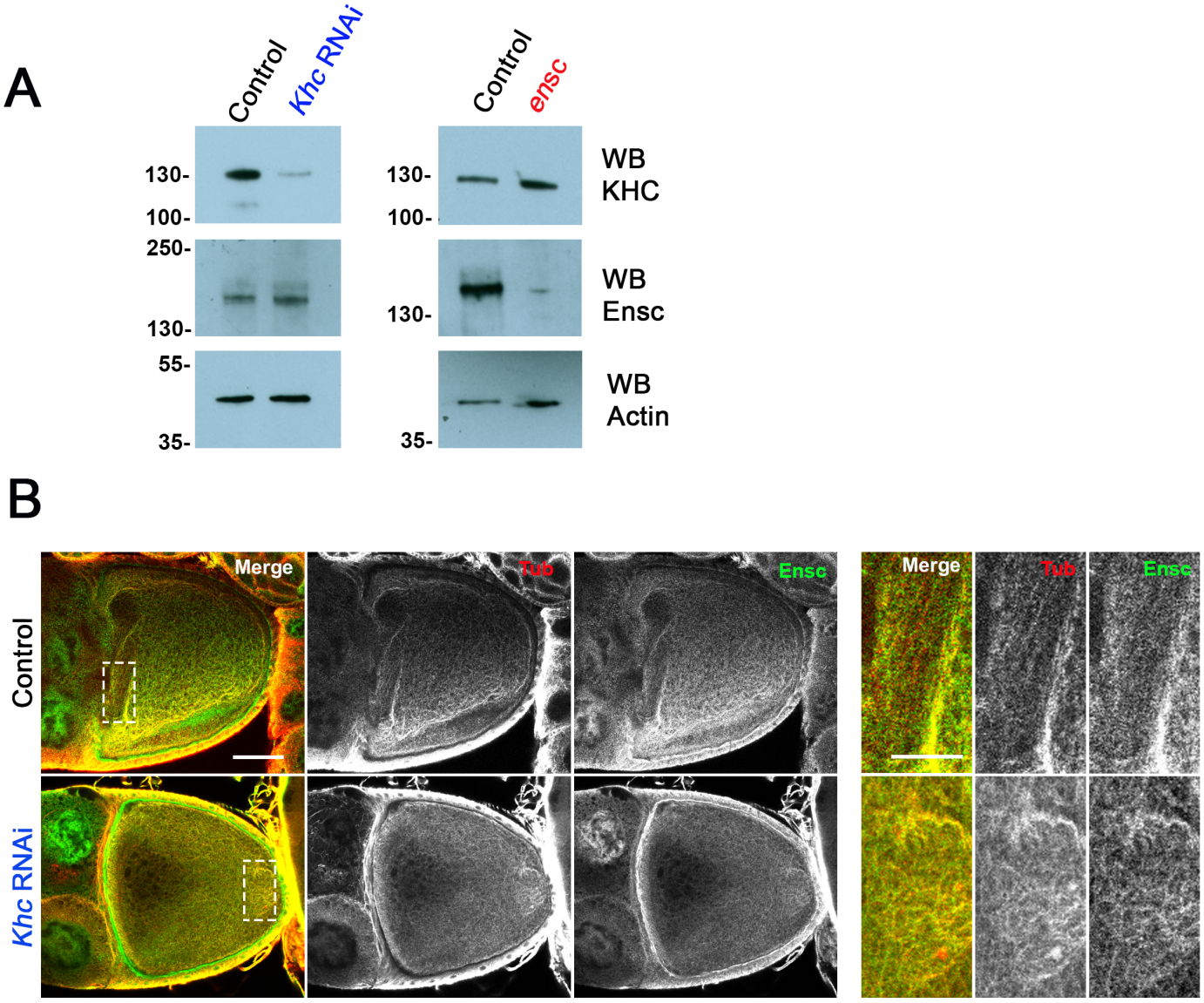

Figure S3. Ensconsin localization in *khc* RNAi oocytes and Western blot analyses.

A) Western blot showing KHC, Ensconsin and actin protein levels in control and *khc* RNAi ovary extracts (left) or in control and *ensc* mutant ovary extracts (right). B) Ensconsin (green in the merge panel and monochrome in the middle panels) and MT localization (red in green in the merge panel and monochrome in the right) panels in WT (top, n=10) and *khc* RNAi oocytes (bottom, n=12). *khc* RNAi oocytes display a loss of the large cytoplasmic MTs bundles but Ensconsin is maintained on the remaining MT cytoskeleton. Insets show an enlarged view of the cytoplasmic MTs. Scale bar 50 μm and 20 μm in the insets.

Development • Supplementary information

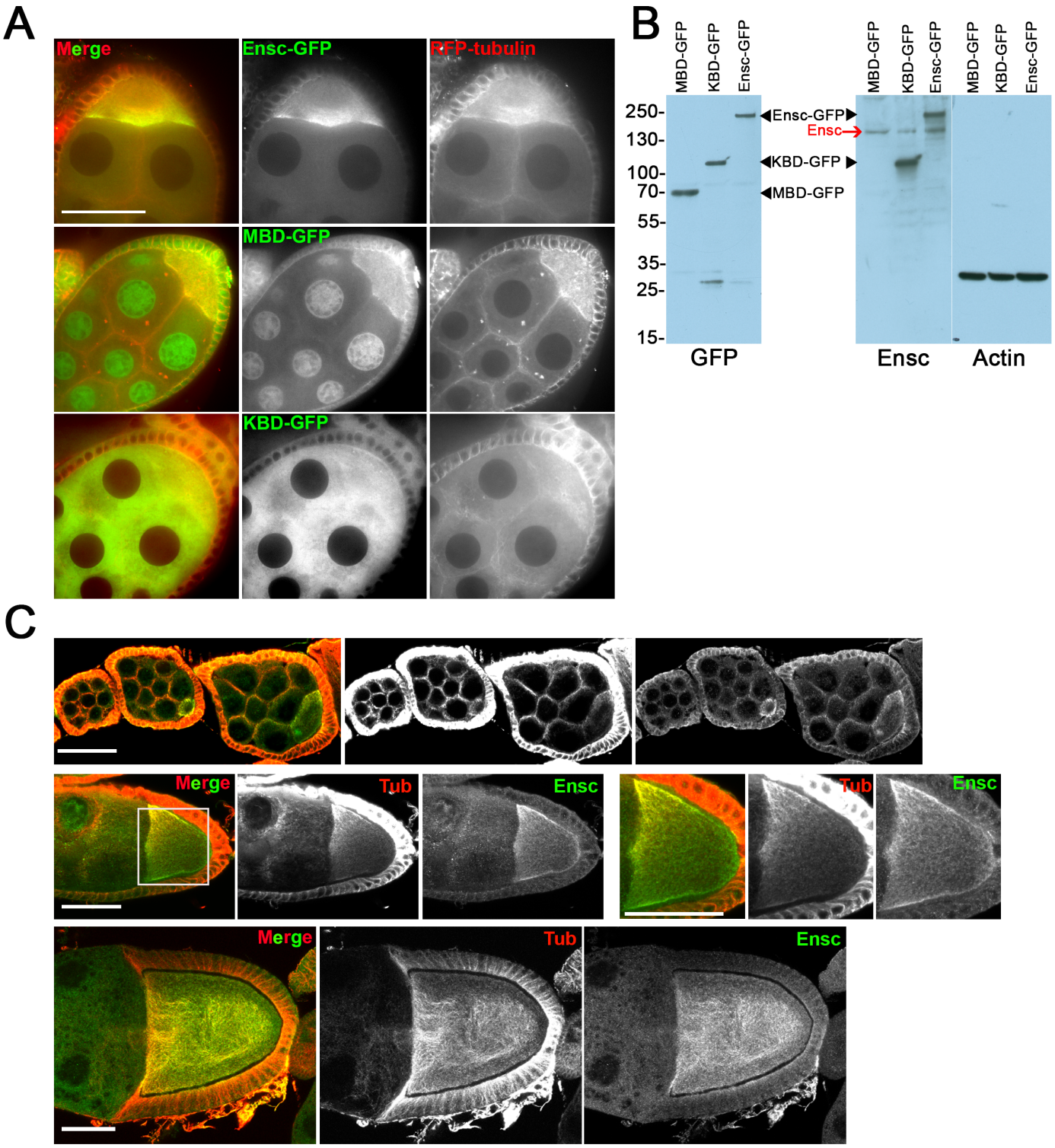

Development • Supplementary information

Figure S4. Localization of Endogenous Ensconsin, Ensc-GFP, KBD-GFP, and MBD-GFP variants in oocytes and in live embryos.

A) Live localization of Ensc-GFP (top), MBD-GFP (middle) and KBD-GFP (bottom) in live early oocytes expressing RFP-tubulin (Red in the merge channel), in a wild type background. Ensc-GFP and MBD-GFP are present on the MT network of the egg chamber and of the epithelial cells. KBD-GFP does not localize on the MT network. Scale bar: 50 μm.

B) Western Blot showing the expression of MBD-GFP, KBD-GFP and Ensc-GFP in ovary extracts from wild type flies. The membrane was probed with anti-GFP antibodies and the three GFP-tagged variants are expressed at similar levels (left). The same membrane was stripped and probed with anti-Ensconsin antibodies raised against the KBD (middle panel). The MBD is not detected. The red arrow indicates the endogenous Ensconsin. The membrane was stripped and probed with anti-actin antibodies (right) as a loading control.

C) Wild type oocytes were permeabilized for 1 h to remove cytoplasmic protein pools (see Methods). They were then fixed and immuno-labelled with an anti-tubulin antibody (red on the left, monochrome elsewhere) and an anti-Ensconsin affinity-purified antibody (green in the left panels, monochrome elsewhere). Scale bars: 50 μm. Note that Ensconsin is first detected in the egg chamber during early stages (top). At later stages, it co-localizes with the polarised MT network (middle panels). The right panels show an enlarged view of the MT cytoskeleton of the corresponding oocyte. During stage 10B, Ensconsin also co-localizes with the MT network involved in ooplasmic streaming (bottom panels).

D) Selected images of a wild type embryo-expressing MBD-GFP as it divides during interphase (at 4:30, left) and during metaphase (8:00, right). E) Selected images of a wild type dividing embryo-expressing KBD-GFP, shown during prophase (1:00, left) and metaphase (4:30, right). The GFP-tagged proteins are green and RFP-tubulin is red in the merge pictures, and they are both monochrome in the other panels. Scale bars: 20 μm. Time is indicated as min:sec. MBD-GFP co-localizes with MTs during mitosis and interphase, but KBD-GFP does not.

Development • Supplementary information

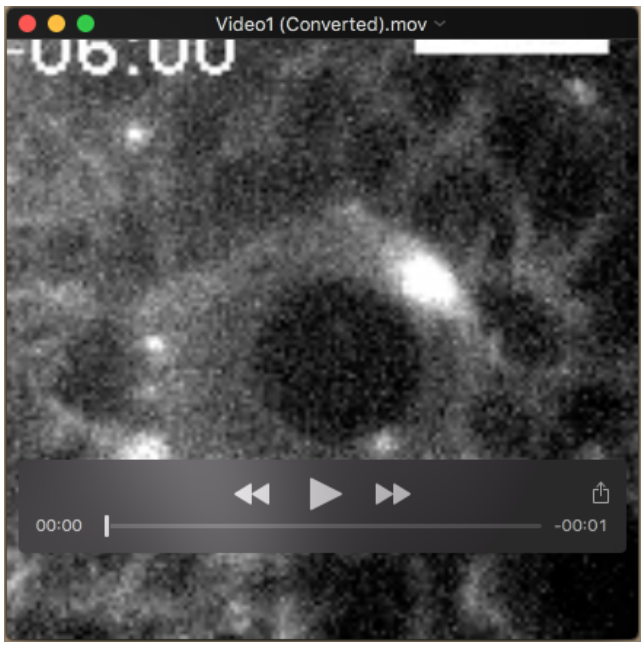

Movie 1. Control dividing NB expressing RFP-tubulin. Scale bar: 10 μm. Time is min:sec.

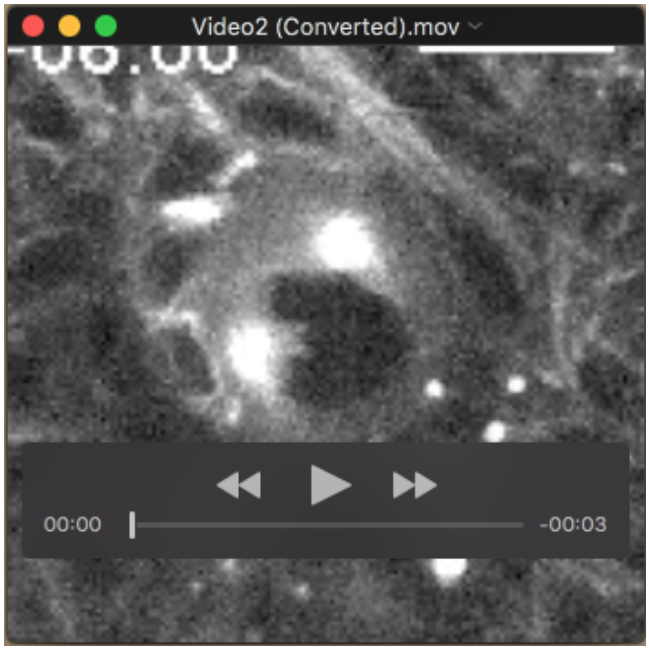

Movie 2. *khc*^{27}/*khc*^{63} mutant NB expressing RFP-tubulin. Scale bar: 10 μm. Time is min:sec.

Development • Supplementary information

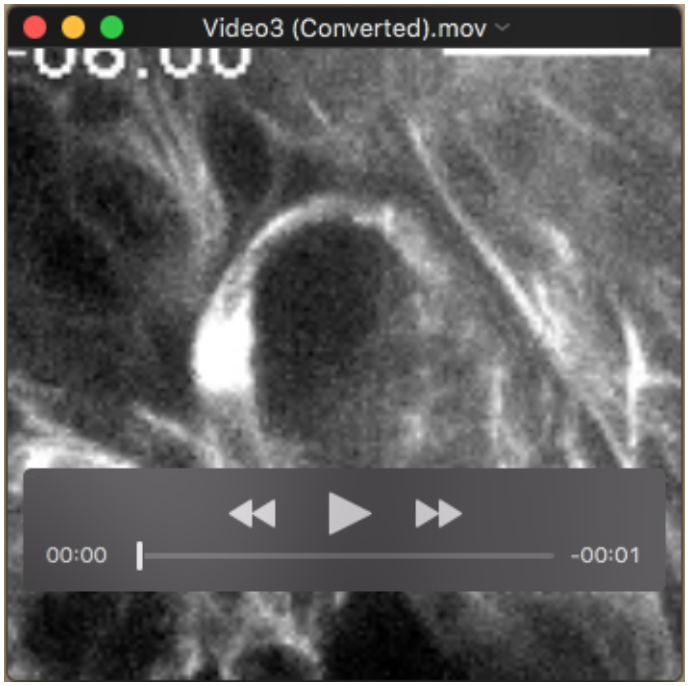

Movie 3. Dividing NB overexpressing Ensc-venus. Scale bar: 10 μm. Time is min:sec.

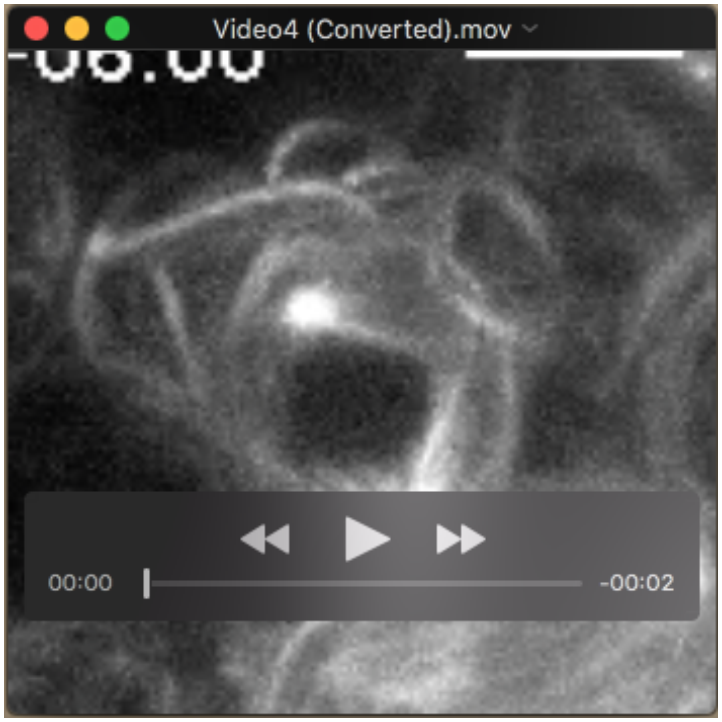

Movie 4. *khc*^{27}*/khc*^{63} mutant neuroblast overexpressing Ensc-Venus during cell division. Scale bar: 10 μm. Time is min:sec.Scale bar: 10 μm. Time is min:sec. See the rescue of the centrosome separation defect.

Development • Supplementary information

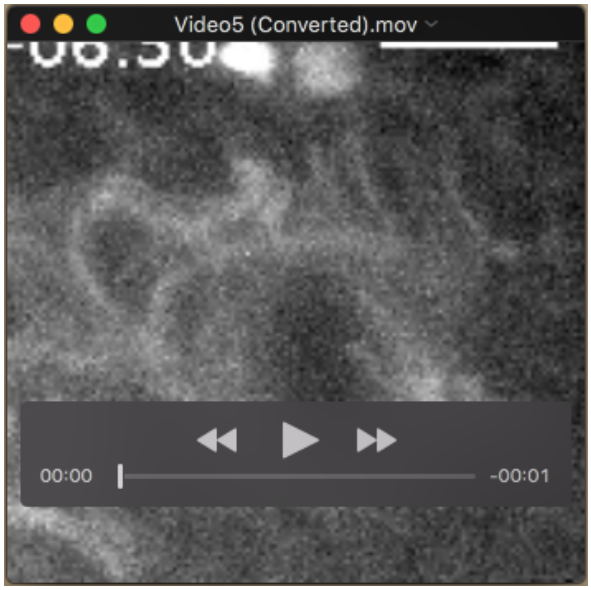

Movie 5. Control dividing NB expressing RFP-tubulin. Scale bar: 10 μm. Time is min:sec.

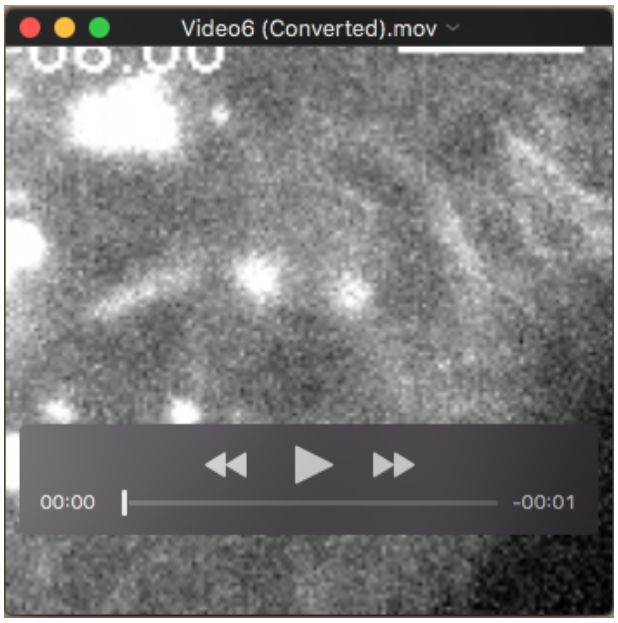

Movie 6. *ensc* mutant neuroblast expressing RFP-tubulin. See the centrosome separation defect. Scale bar: 10 μm. Time is min:sec.

Development • Supplementary information

Movie 7. *ensc* mutant NB expressing RFP-tubulin (red in the merge panel and monochrome in the middle panel) and MBD-GFP (Green in the middle panel, and monochrome in the right panel). There is no rescue of the interphase centrosome separation defect. Scale bar: 10 μm. Time is min:sec.

Movie 8. Squashed *ensc* mutant NB expressing RFP-tubulin (red in the merge panel and monochrome in the middle panel) and KBD-GFP (green in the merge panel, and monochrome in the right panel). The interphase centrosome separation defect is restored. Scale bar: 10 μm. Time is min:sec.

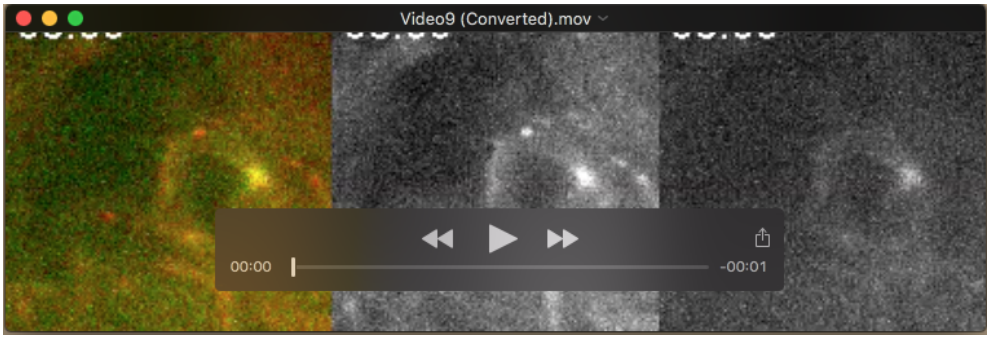

Movie 9. *ensc* mutant NB expressing RFP-tubulin (red in the merge panel and monochrome in the middle panel) and full length Ensc-GFP (green in the merge panel, and monochrome in the right panel). Interphase centrosome separation is restored. Scale bar: 10 μm. Time is min:sec.

Development • Supplementary information